2012

Submillisecond-response Blue Phase Liquid Crystals For Display Applications

Kuan Ming Chen
University of Central Florida

SUBMILLISECOND-RESPONSE BLUE PHASE LIQUID CRYSTALS FOR DISPLAY APPLICATIONS

by

KUAN-MING CHEN
B.S. in Electronics Engineering, National Chiao-Tung University, Taiwan, 2001
M.S. in Graduated Institute of Electronics Engineering, National Taiwan University, Taiwan, 2003

A dissertation submitted in partial fulfillment of the requirements
for the degree of Doctor of Philosophy
in the College of Optics and Photonics
at the University of Central Florida
Orlando, Florida

Spring Term
2012

Major Professor: Shin-Tson Wu

ABSTRACT

With exploding growth of information exchanges between people, display has become indispensable in our daily lives. After decades of intensive research and development in materials and devices, and massive investment in manufacturing technologies, liquid crystal display (LCD) has overcome various obstacles and achieved the performance we need, such as wide viewing angle, high contrast ratio, and high resolution, etc. These excellent performances make LCD prevailed in every perspective. Recently, with the demands of energy conservation, a greener LCD with lower power consumption is desired. In order to achieve this goal, new energy-effective driving methods, such as field sequential color display, have been proposed. However, in order to suppress color breakup the LC response time should be faster than 1 ms. To overcome this challenge, various fast-response liquid crystal modes, such as thin cell gap, low viscosity materials, overdrive and undershoot voltages, polymer stabilization, and ferroelectric liquid crystal, are under active investigations. Among these approaches, blue phase liquid crystal (BPLC) shows a greater potential with less fabrication limitations.

In this dissertation, the feasibility of polymer-stabilized blue phase liquid crystal for display applications is explored starting from the building blocks of the material system, polymer-stabilization processes, test cell preparations, electro-optical (EO) properties, to suggested approaches for further improvements.

Because of the nature of blue phase liquid crystals, delicate balance among system components is critically important. Besides the properties of each composition, the preparation process also dictates the EO performance of the self-assembled nano-structured BPLC composite. After the preparation of test cells, EO properties for display applications are investigated and results described. Approaches for further improvements of the EO properties are also suggested in the final part of this dissertation.

ACKNOWLEDGMENTS

I would like to express my gratitude to those who have made contributions to this work and who have offered supports during my study and research.

First of all, I would like to thank my advisor Prof. Shin-Tson Wu for his guidance, encouragement and support during my Ph. D study. I treasure the opportunity of working in such a great group led by Prof. Wu.

I am also grateful to all of my committee members Prof. Patrick L. LiKamWa, Prof. David J. Hagan and Prof. Jiyu Fang for their supports and valuable comments.

In addition, I would also like to thank all my colleagues, especially Dr. Sebastian Gauza, Dr. Hongwen Ren, Dr. Haiqing Xianyu, in the Photonics and Display group at CREOL, for the valuable discussions, inspiration and help while working with blue phase liquid crystals.

Moreover, I would like to thank Air Force Office of Scientific Research (AFOSR), Industrial Technology Research Institute (ITRI, Taiwan), AU Optronics Corp. (AUO, Taiwan) for their financial support of my study and research at University of Central Florida.

TABLE OF CONTENTS

LIST OF FIGURES

LIST OF TABLES

CHAPTER 1: INTRODUCTION

1.1 Thesis Structure

Liquid crystal is a material state between isotropic liquid and solid crystal. It possesses many properties at the same time which are only either found in liquids or solids. For example, liquid crystal can flow like liquids and have optical birefringence like crystals. Besides these characteristics, liquid crystal could also interact with electric or optical field. Therefore, liquid crystal has been widely used for electro-optic and optical applications.

Based on their properties and formations, liquid crystals can be roughly classified into three groups: thermotropic, lyotropic and polymeric liquid crystals. Each type of liquid crystals has a wide variety of categories and applications. In this thesis, we will focus mainly on the blue phase liquid crystal which is a part of chiral liquid crystals in the thermotropic liquid crystal system. Discussions will cover from the observations, the properties of blue phase liquid crystal materials, and then, the electro-optic phenomena. At the final part, future research directions of blue phase liquid crystals for display applications will be discussed.

1.2 Chirality and Liquid Crystals

Chirality is a commonly seen characteristic in nature. An object or a system without mirror symmetry is called chiral. The most universally recognized examples are human hands.

Chirality is also easily observed in the molecular structures with same atomic compositions but in slightly different arrangements. Fig. 1.1 presents two pair of chiral examples as human hands and amino acid.

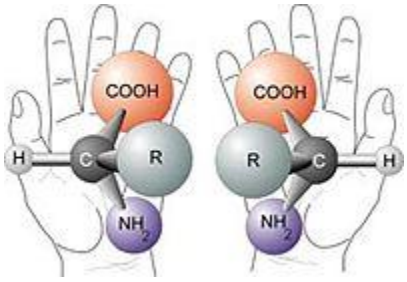

Figure 1.1 Chiral pairs as human hands and amino acid. [1]

In liquid crystals, chirality is also an easily observed characteristic. A chiral liquid crystal exists in a compound which is either composed of molecules with chiral structures or induced by adding chiral molecules into an achiral liquid crystal system. Because of the chirality, chiral liquid crystals possess many distinct and interesting properties. Different from commonly known nematic liquid crystals, in a chiral liquid crystal system the mirror symmetry disappears, the translation symmetry is reduced, and additionally, the spatial periodicity shows up. These basic differences complicate the minimum Landau free energy states in three dimensions and ultimately lead to a new liquid crystal state. As a result, new properties that are different from the nematic liquid crystal system manifest.

Depending on applications, different properties of liquid crystal systems could be employed, such as thermal transition (in thermotropic liquid crystal) or molecular interaction (in lyotropic liquid crystal). Among these features, electric field-induced LC director reorientation is commonly used in display and photonic devices. Here, we focus on the electric field-induced refractive index change. Generally speaking, when a system composed of polar groups is under

the influence of an electric field, the dielectric polarization density *(P)* can be described as:

$$P = \varepsilon_0 \chi E \,, \tag{1.1}$$

where ε_0 is electric permittivity in free space, χ is the electric susceptibility, and E is the electric field. In a general system, the electric susceptibility χ is a nonlinear factor to the electric field E, which can be expressed as

$$\chi = \chi^{(1)} E + \chi^{(2)} EE + \chi^{(3)} EEE + \ldots, \tag{1.2}$$

In a system which lacks of inversion symmetry or centrosymmetry, the linear term of the electric susceptibility dominates, which is referred as the Pockels effect. [2] However, in a symmetric system, like chiral systems, the linear term vanishes and the $\chi^{(3)}$ term dominates. The rest of the susceptibility terms still exist but in a relative small value. As a result, the electric displacement *(D)* can be written as

$$D = \varepsilon_0 E + P = \varepsilon_0 \left(E + \chi^{(1)} E + \chi^{(3)} EEE + \ldots \right), \tag{1.3}$$

From this expression, the relative permittivity (ε_r) can be found as

$$\varepsilon_r = 1 + \chi^{(1)} + \chi^{(3)} EE + \ldots. \tag{1.4}$$

From Maxwell equations, the refractive index *(n)* of the system can be approximated as

$$n = \sqrt{\varepsilon \mu} \cong 1 + \chi^{(1)} + \frac{1}{2} \frac{\chi^{(3)} E^2}{1 + \chi^{(1)}} + \ldots. \tag{1.5}$$

The electric-field-induced refractive index change (δn) of the system is mainly proportional to the square of the electric field, which is commonly known as Kerr effect [2]:

$$\delta n = \lambda K E^2 \,. \tag{1.6}$$

For many organic materials studied, the Kerr constant *(K)* is very small. For example for nitrobenzene, its K~4.4 pm/V^2. A small Kerr constant leads to a small induced refractive index unless the applied electric field is large.

1.3 Cholesteric Liquid Crystals

The early articles of chiral liquid crystals can be traced back to an Austrian botanical physiologist, Friedrich Reinitzer, in 1888. During his examinations over various derivatives of cholesterol, besides the already observed color effect above melting point, he found that cholesteryl benzoate has two melting points. After more observations and discussions with Otto Lehmann and von Zepharovich, he described three important features of a cholesteric liquid crystal: 1) existence of two melting points, 2) reflection of circularly polarized light, and 3) ability to rotate the polarization direction of the incident light. [3][4]

From experimental observations and theoretical explorations, cholesteric liquid crystal can be regarded as a structure with a helical axis as shown in Fig. 1.2. In the illustration, liquid crystal directors gradually rotate in an angle along the helical axis. Therefore, a distance along this helical axis can be defined as a pitch (P_0) when the liquid crystal director ($\hat{n}$) rotates back to its original direction.

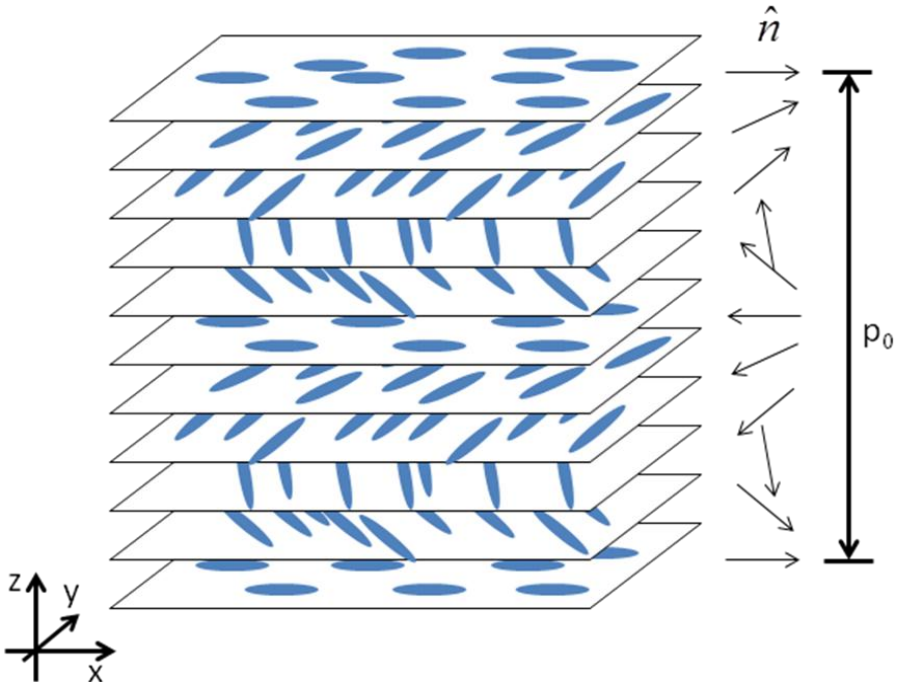

Figure 1.2 Molecular structure in a cholesteric liquid crystal. [5]

Layer-like structures are formed perpendicular to the helical axis in a cholesteric liquid crystal. Fig. 1.3 presents the cross-section view along the helical axis of a polymerized cholesteric liquid crystal. [6] The pitch length of the cholesteric liquid crystal is about 1μm and the helical axis is in the vertical direction. The inset is the transmittance spectrum of this layered structure.

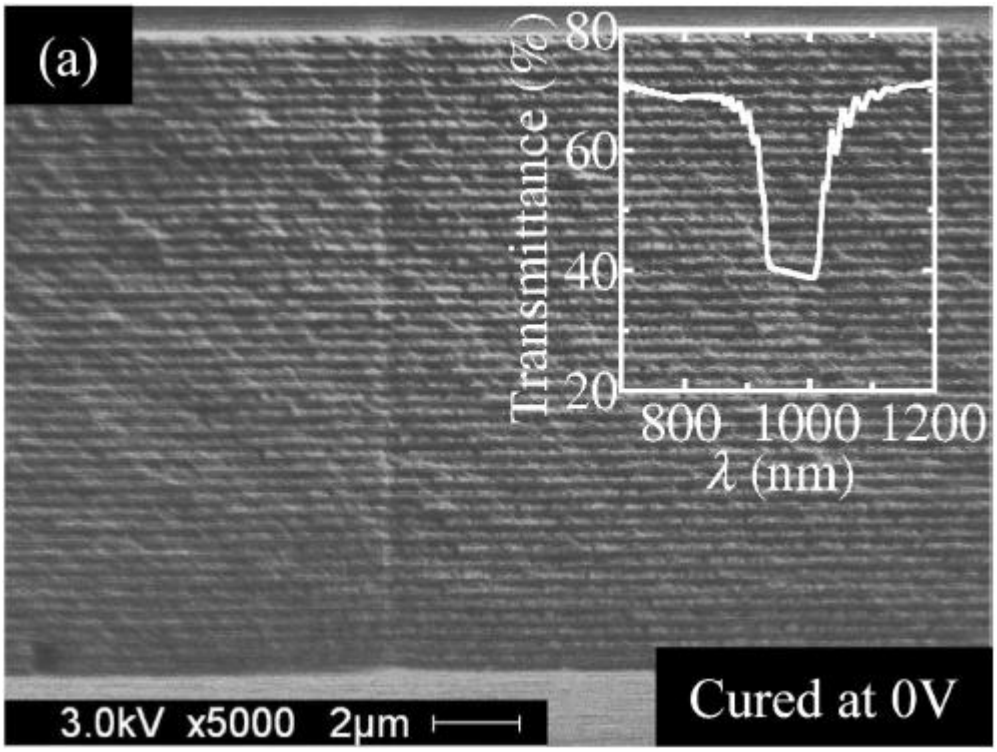

Figure 1.3 Scanning electron microscopy of cholesteric liquid crystal layer structures. [6] (Reprinted by permission from SID, © 2008)

Because of this helical arrangement, the refractive index along the helical axis is changed periodically. This periodic refractive index distribution makes cholesteric liquid crystal an optically active medium reflecting the incident light in certain bandwidth, which leads to distinct colors. Fig. 1.4 shows the calculated reflection spectrums when the birefringence (Δn) of the liquid crystal host is 0.2 and 0.4, respectively. [7] The center wavelength λ_o of the reflection band can be obtained from [8]

$$\lambda_o = \tilde{n}P, \tag{1.7}$$

where $\tilde{n}$ is the averaged refractive index of the liquid crystal and P is the pitch length. The

bandwidth $\Delta\lambda$ of the reflection band can be found as

$$\Delta\lambda = \Delta nP\,, \tag{1.8}$$

where Δn is the birefringence of the liquid crystal. Depending on the handedness of the helical structure, either right- or left-handed circular polarized incident light will be reflected. Meanwhile, the incident light with a polarization of opposite handedness will transmit through. Thus, the maximum reflectance in Fig. 1.4 is about 50% because the cholesteric liquid crystal is only optically active to one polarization of the incident light.

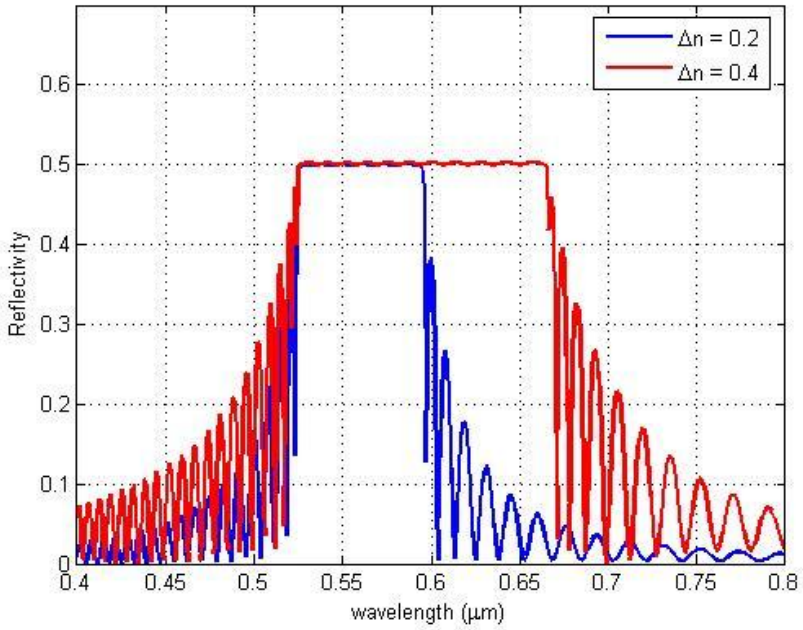

Figure 1.4 Calculated reflection spectrum of a cholesteric liquid crystal. [7]

Fig. 1.5(a) shows the texture of a cholesteric liquid crystal under polarizing optical microscope and Fig. 1.5(b) is the corresponding reflection spectrum. [6]

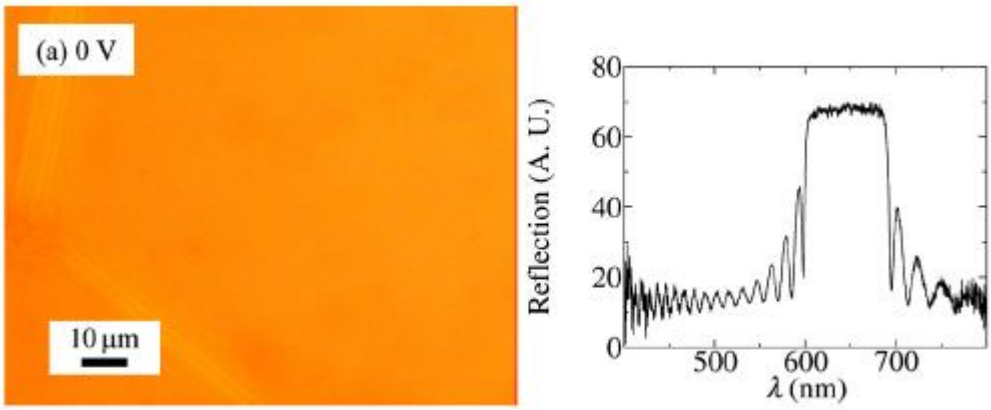

(a) (b)

Figure 1.5 (a) Texture of a cholesteric liquid crystal under polarizing optical microscope. (b) The corresponding reflection spectrum. [6] (Reprinted by permission from SID, © 2008)

1.4 Blue Phase Liquid Crystals

In the beginning of 20th century, O. Lehmann discovered an intermediate phase in a narrow temperature interval during the isotropic liquid and the cholesteric transition, which is different from isotropic liquid and cholesteric state. [9][10] Lehmann's observations were confirmed by later investigators, especially by Gray, who called this intermediate phase the "blue phase". [11] Moreover, by calorimetric [12][13] and optical [14][15] measurements two or even three stable phases (called BPI, BPII, and BPIII) were found within this very narrow temperature interval. Continuous to 1980s, intensive works based on theories from different perspectives [16], gradually reveal and explain the stable geometry of the BP states.

After decades of experimental and theoretical investigations, the commonly accepted

crystalline structures in the blue phase states are body center cubic (bcc) structure for BPI, simple cubic (sc) structure for BPII, and an unknown amorphous close to isotropic state for BPIII. [17][18] The thermal scheme of the blue phase states is illustrated in Fig. 1.6. [16] While temperature increases, BP phases appear sequentially from BPI to BPIII between the cholesteric and the isotropic states.

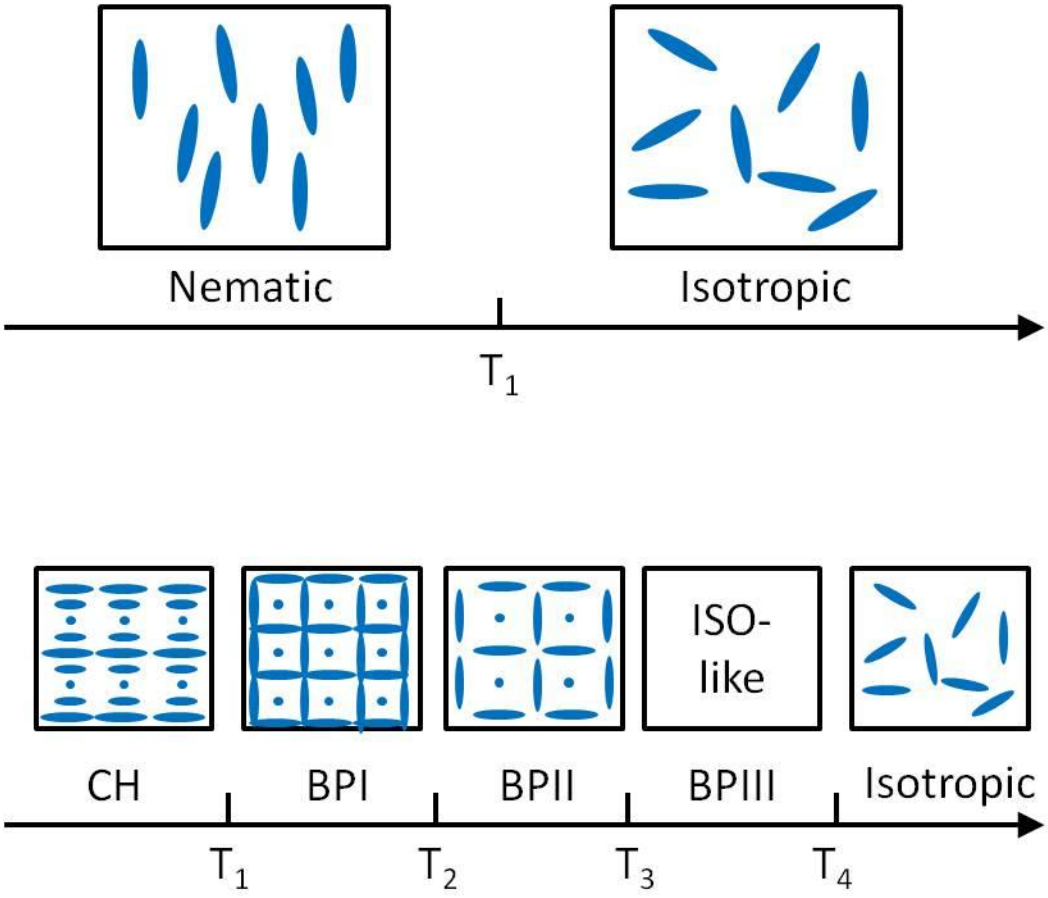

Figure 1.6 Thermal schemes of the blue phase states. [16]

In the cubical model of the blue phase structures, to satisfy the minimum free energy configuration the arrangement of the liquid crystal directors is considered as a double-twisted cylinder formation illustrated in Fig. 1.7. [17]

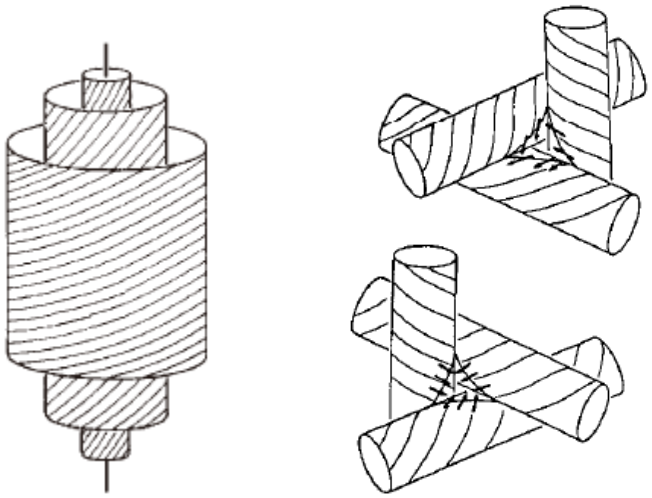

(a) (b)

Figure 1.7 (a) Scheme of local directors in a double-twisted cylinder. (b) Stacking of double-twisted cylinders and frustrated defects. [17] [77] (Reprinted by permission from Taylor & Francis: Molecular Crystals and Liquid Crystals, © 1991)

In this double-twisted cylinder formation, liquid crystal directors rotate spatially about any radius. However, filling these double-twisted cylinders into a three dimensional space is topologically impossible. Defects, as illustrated in Fig. 1.7(b), between the intersections of the cylinders become the key to relieve the strain. [18]-[23] As a result, blue phase state is a delicately balanced system of the crystalline and defect structures. Fig. 1.8 presents the cubical crystalline stacking of the double-twisted cylinders and the corresponding defect lines (disclination lines) in different blue phase states.

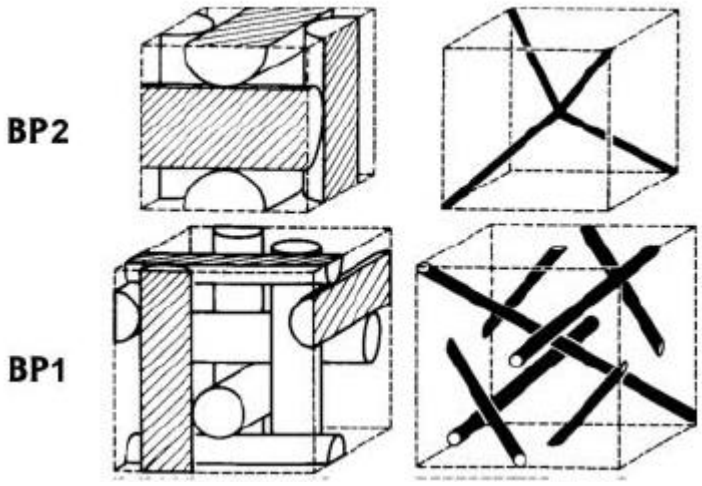

(a) (b)

Figure 1.8 (a) Scheme of double-twisted cylinders in the cubical crystal lattice. (b) The corresponding frustrated defect lines. [77] (Reprinted by permission from Taylor & Francis: Molecular Crystals and Liquid Crystals, © 1991)

Because of the nature as a defect balanced system, the existence of the blue phase state is limited within a very narrow range about few degrees. Under this limited stable range, blue phase liquid crystal is only investigated as a scientific interest. Practical application based on blue phase liquid crystals is hardly imagined. As a result, approach to widen the stable temperature range is the key for blue phase liquid crystals to prevail. To overcome this obstacle, several approaches have been proposed. First, Coles et al starts from the molecular engineering perspective by creating a new molecular structure as shown in Fig. 1.9. [24]

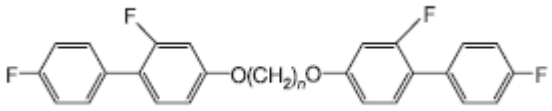

Figure 1.9 Molecular structure proposed by Coles et al. (Reprinted by permission from Macmillan Publisher Ltd: Nature, © 2005)

This type of molecule has a rigid biphenyl core in both ends and a flexible alkyl chain in the middle connecting these two end groups. The number of carbon (n) in the middle alkyl chain is from 7 to 9. A stable wide temperature range in blue phase state, starts from 16.5˚C to 57.7˚C, has been reported. Microscopically speaking, the flexible long alkyl chain allows the rigid end cores to be orientated in any direction in order to satisfy the blue phase stacking structure as shown in Fig. 1.8. Therefore, even over a wide span of temperature, the molecular arrangements can still be kept in the blue phase structure. However, the dipole of this type of molecule is small so that a high electric field (14V/μm) is required to induce the electro-optical response.

Another family of new molecular structure for widening the stable temperature range is proposed by Yoshizawa et al. [25] This type of mega-molecule has two long chains connected to the central phenyl ring and the whole molecular structure is in a T shape. A relatively wide blue phase temperature range of about 13 degrees, from 15˚C to 28˚C, is observed during the cooling process. However, this type of mega-molecule has other concerns in practical applications such as, small dipole, high viscosity, miscibility to regular liquid crystals, etc.

The second approach proposed by Yoshida et al is to dope blue phase liquid crystals with gold nanoparticles. [26] After doping gold nanoparticles in blue phase liquid crystal mixture by sputtering, blue phase temperature range increases from 3 degrees to 9 degrees during the

cooling process. Similar approach by mixing blue phase liquid crystal mixture with surface-functionalized CdSe nanoparticles is reported by Karatairi et al. [27] It is believed that the doped nanoparticles are attracted to the defect lines (disclination lines). As a result, the penalty of the system's free energy for the formation of defect lines decreases. Blue phase state, therefore, can be stabilized over a wide temperature range.

The third approach is the polymer stabilization method proposed by Kikuchi et al. Until now, this is the most promising approach to widen the stable blue phase temperature range for practical applications. In 2002, Kikuchi et al proposed this breakthrough approach which opens a new door for practical applications. [28] To realize the stabilization of the liquid crystal molecules in blue phase states, polymer networks are introduced into the system. With a properly optimized process, polymer network is believed to form in the defect volume, i.e., alone the disclination lines as Fig. 1.8 shows. After the formation of the polymer networks in the blue phase structures, the stable temperature range is extended over 60 degrees. Besides this wide stable temperature, such a polymer-stabilized blue phase liquid crystal also keeps a very fast response time as observed in the regular blue phase liquid crystals.

However, some issues remain a concern for the polymer-stabilized blue phase liquid crystals to be utilized in displays, for examples, high operating voltage and hysteresis. In the issue of the high driving voltage, different approaches by improving the material compositions or the device structures have been proposed by different groups. [29]-[35] These useful methods for reducing operation voltage will be discussed in this dissertation. Until now, the practically realized operating voltage is ~40V_{rms} unless protrusion electrodes are considered [35]-[37] Another concern is hysteresis. The hysteresis problem has been tackled for decades in liquid

crystal/polymer composites such as polymer-dispersed liquid crystal (PDLC) system. Unfortunately, hysteresis is also present in blue phase liquid crystal system. [38] Further work to reduce hysteresis is still under active investigations. [39]-[40]

1.5 Liquid Crystal Displays

Nowadays, flat panel display has prevailed in every corner, from small-size panels in personal watches or cellular phones, to mid-size monitors in personal computers to large-size TVs or public advertising boards. Among various display technologies, liquid crystal display (LCD) based on nematic liquid crystals is the most popular one. With the rapid growth of LCD technology, light weight, low power consumption, high resolution, fast response, vivid color performance and many other features make LCD indispensable in our daily life.

Generally speaking, a LCD panel is composed of a light source (backlight), driving circuits (TFTs), a liquid crystal layer, polarizers and RGB color filters as shown in Fig. 1.10.

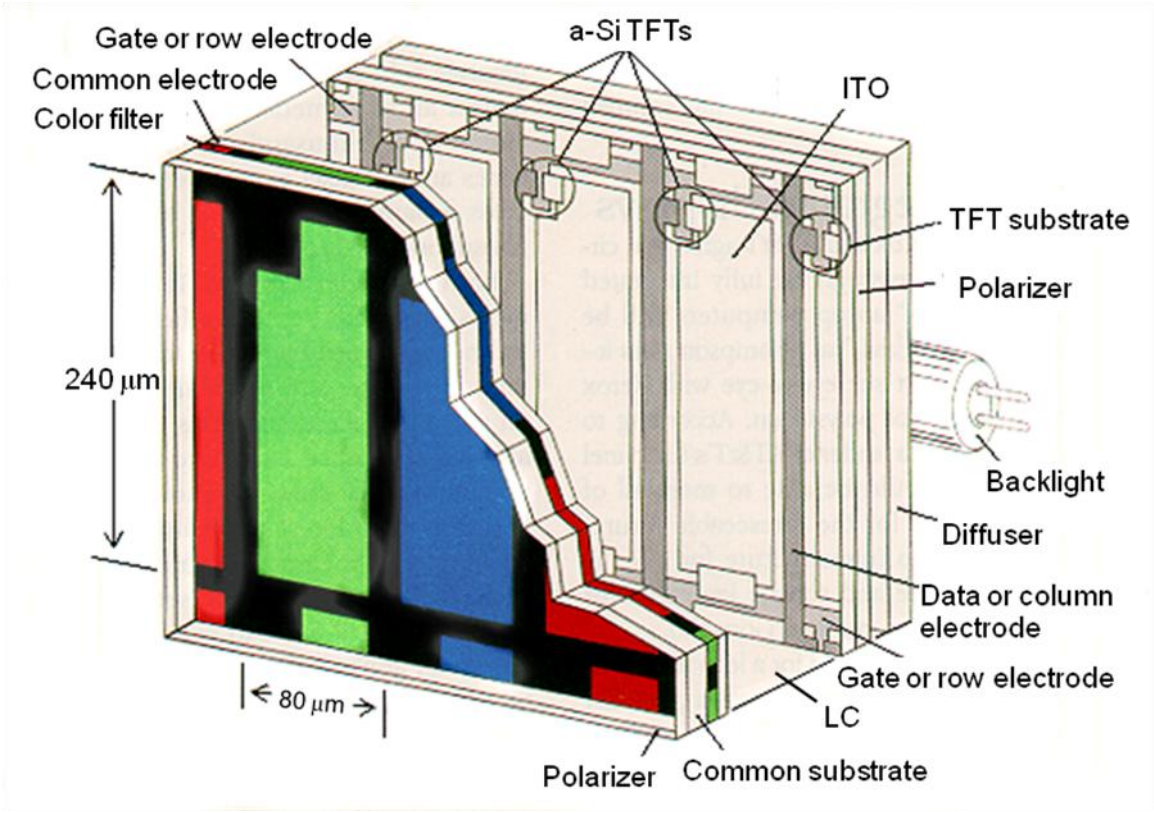

Figure 1.10 Device structure of a transmissive TFT LCD pixel with RGB sub-pixels.

To achieve the abovementioned performances, effort to improve each component is still ongoing. Among these improvements, the liquid crystal layer has the greatest impact and also evolves dramatically. In the first LCD prototype demonstrated by RCA in 1960s, dynamic scattering mode was employed. However, the material stability, contrast ratio, and power consumption are big concerns for this operation mode. In early 1970s, twisted nematic (TN) mode was invented. [41] After TN, due to different applications, the liquid crystal operation mode evolved rapidly into super-twisted nematic (STN) for high information content, in-plane switching (IPS) for wide viewing angle [42][43], multi-domain vertical alignment (MVA) for high contrast and wide-view [44][45], and fringing field switching mode (FFS) for wide viewing

angle and high transmittance [46]. Currently, because the energy consumption problem becomes an urgent issue, the replacement of the backlight unit from cold cathode fluorescent lamps (CCFL) to light emitting diodes (LED) has been implemented. Furthermore, the needs for new liquid crystal operation mode also become critical to enable a more energy efficient display driving, such as the color sequential operation. [47] Compared to the conventional nematic liquid crystals, blue phase liquid crystal has a 10X faster response speed at around hundreds of microsecond. This fast response time makes blue phase a strong contender as next-generation display technology.

Besides fast response time, some other advantages of blue phase liquid crystals can also be realized, such as alignment layer free and cell gap insensitivity if in-plane switching electrodes are used. Figure 1.11 illustrates conventional cell assembly process of a TFT-LCD panel.

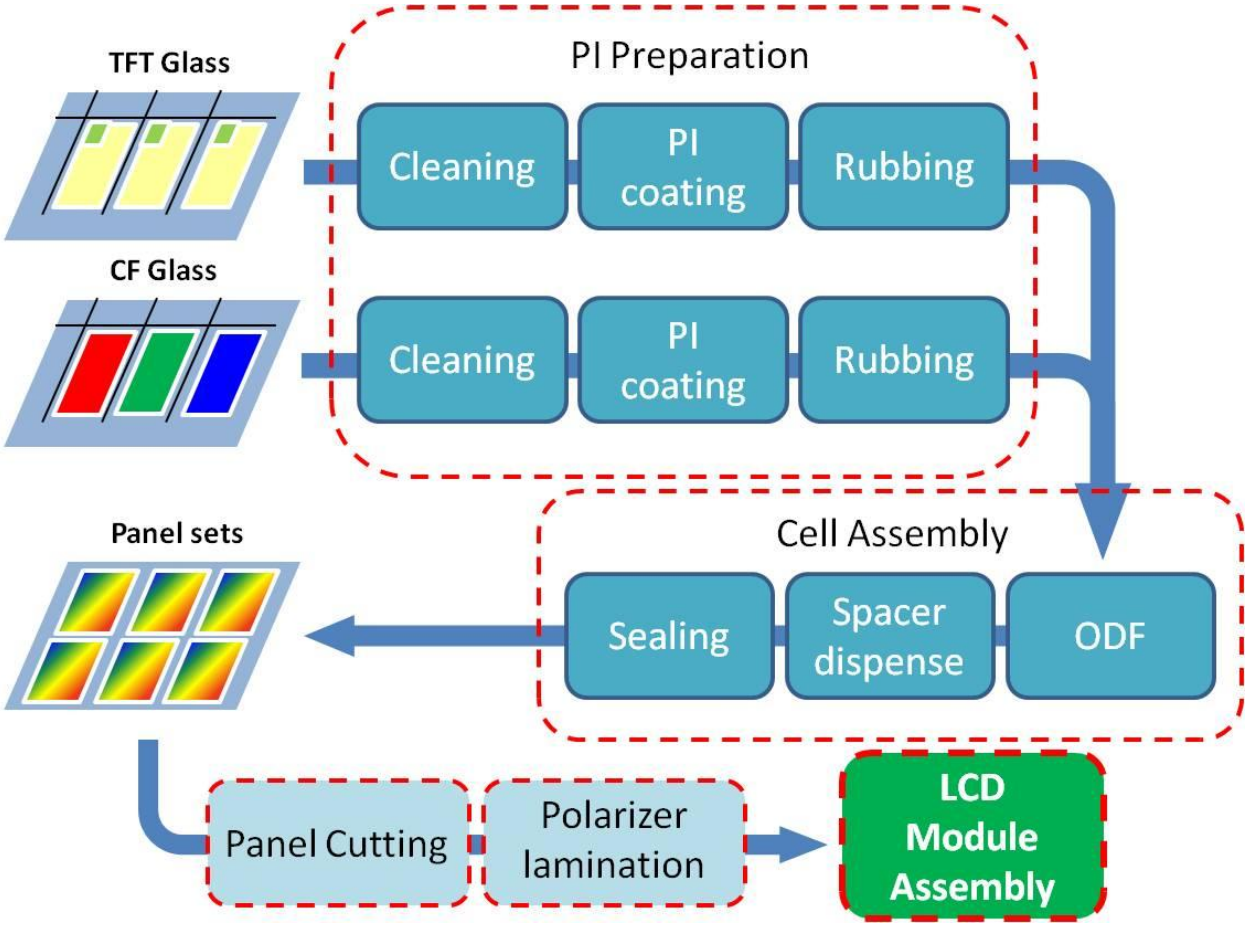

Figure 1.11 Cell assembly process of a TFT LCD panel.

Before the cell assembly process, the bottom and the top glass substrates are prepared with TFT structures and RGB color filters (CF), respectively. During the cell assembly process, both TFT and CF substrates are first coated with a layer of polyimide (PI) and then rubbed by a nylon cloth in a given direction. These two procedures regulate the arrangement of the liquid crystal molecules and help to align liquid crystal molecules in a designated direction. After the above processes, liquid crystal mixture is injected to the gap between these two glass substrates by one-drop-fill (ODF) method. Spacer balls are also spread at the same time to control the cell gap (liquid crystal layer thickness) between these two substrates. In the end of the cell assembly

process, these two substrates are sealed by a UV curable sealant and cut into proper sizes for next polarizer lamination step.

Because of the self-assembly nature in blue-phase liquid crystals, the cell assembly process can be greatly reduced by skipping the PI coating and the rubbing processes. Furthermore, the electrode configuration gives another advantage to simplify the fabrication process. Generally speaking, the thickness and uniformity of the liquid crystal layer in a conventional TFT-LCD panel are very critical. Issues such as brightness uniformity, dark state uniformity, color performance, moiré, would show up when the thickness uniformity is slightly off. Based on the operation of a blue-phase liquid crystal, an IPS electrode configuration is preferred. Due to the limited penetration depth of the effective electric field induced by the electrodes on the same substrate, the performance of the blue-phase liquid crystal is not sensitive to the cell gap variation when the LC layer is thicker than a certain value, say 3-4 μm. [48] This tolerance relieves the requirements of the thickness control in the liquid crystal layer and the flatness uniformity of the glass substrates which are difficult to control precisely for a large-panel LCD TV.

1.6 Summary

Liquid crystal is a fascinating matter that possesses many special properties at the same time. Especially in the chiral liquid crystal systems, various optical active properties, such as selective reflections in color and polarization, can be utilized for many applications. In this dissertation, the discussion will start from the selection and establishment of blue phase liquid crystal systems based on different liquid crystal materials in Ch. 2. Then, the characterization of

the electro-optical properties of a properly chosen blue phase liquid crystal system follows in Ch. 3. In Ch. 4, an easy and most promising blue phase range widening approach, the polymer stabilization method, will be utilized to this selected system. Different optimization procedures will be performed according to the initial state of the systems. In the aspect for display applications, voltage induced transmittance, response time, and the hysteresis issue in polymer-stabilized blue phase liquid crystal will be addressed and analyzed. In the last part of Ch. 4, the roadmap for further improvements in voltage reduction for display applications will be presented.

CHAPTER 2: MATERIALS AND CHARACTERIZATION METHODS

2.1 Material Systems

In this chapter, the LC components required for forming blue phase liquid crystal system is reviewed. In general, to obtain a chiral liquid crystal system either single structure mesogens of a chiral nature or chiral molecules doped-achiral LC host are needed. The host material will be discussed first, followed by chiral molecules doped-nematic liquid crystals. Finally, we will introduce some intrinsically chiral liquid crystals for which blue phase can be observed without additional dopants.

2.1.1 High Birefringence Liquid Crystals

Several commercially available high birefringence mixtures were studied for their suitability as a host LC for blue phase material. In this section we investigate some Merck E, TL and BL series of LC mixtures and high dielectric anisotropy TEB-series nematic LC mixture from Slichem.

2.1.1.1 High Birefringence Merck E-series

First, we start from the most popular liquid crystal mixtures, the E-series. E-series liquid crystals are used in various applications. For example, E44 was widely used in optical phase modulator, [49] [50] phase grating, [51] focusing lens, [52] [53] spatial light modulator (SLM),

[54] polymer/liquid crystal composite, [55] [56] cholesteric liquid crystal laser, [57] and etc. As reported in early works, E44 liquid crystal mixture has a cyano polar group [58]. The major compounds in E44 have a biphenyl core and a cyano end group as illustrated in Fig. 2.1.

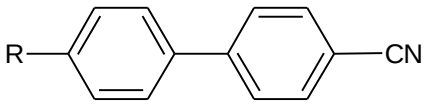

Figure 2.1 Major structure of compounds in E44. R is alkyl chain.

2.1.1.2 High Birefringence Merck TL-series

The second type of liquid crystal used here is the TL-series. The TL-series liquid crystal, such as TL213, is commonly used in the polymer-dispersed liquid crystal (PDLC) system [59] [60] or phase grating. [61] As reported in prior arts, superfluorinated liquid crystal mixture (TL213) and monomer mixture (PN393, Merck) can form a sponge like liquid crystal/polymer composite which increases the light scattering effect and is beneficial to the PDLC systems. [62][63]

2.1.1.3 High Birefringence BL-series

The third type of liquid crystal is the BL-series, which is also used in the PDLC system but with a higher birefringence. For example, BL038 with a birefringence of 0.27 is commonly seen in holographic PDLC system, [64] PDLC grating, [65] [66] tunable lens, [67] and beam steering device. [68]

2.1.1.4 High Birefringence TEB-series

The last liquid crystal mixture, TEB300, is from TEB-series by Slichem, which has a

higher dielectric anisotropy. This nematic liquid crystal is also usually used for PDLC system. [69] The material parameters of the liquid crystal mixture from each series are listed in Table 2.1, respectively.

Table 2.1 Material parameters of liquid crystal mixtures.

Parameters	E-series	TL-series	BL-series	TEB-series
Mixture	E44	TL213	BL038	TEB300
Viscosity (cSt, 20˚C) /(mm^2s^{-1},20˚C)	47	49	72	89
Δε (1kHz, 20˚C)	16.8	5.7	16.4	29.3
ε// (1kHz, 20˚C)	22	10	21.7	10.3
Δn (589nm, 20˚C)	0.2627	0.239	0.2720	0.166
n_o (589nm, 20˚C)	1.5277	1.527	1.5270	1.677
$K_{11}/10^{-12}$N (20˚C)	15.5	16.8	13.7	7.4
$K_{33}/10^{-12}$N (20˚C)	28.0	22.0	27.7	12.6

2.1.2 Chiral Dopants

To induce chirality in nematic liquid crystal mixtures, chiral agent is a key component. Here, we will discuss some commonly used chiral agents. Fig. 2.2 depicts the molecular structure of the chiral agents discussed in this work.

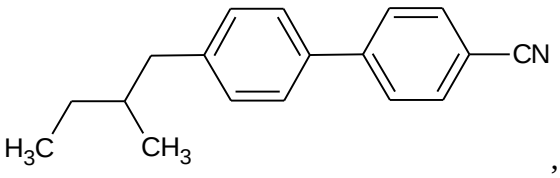

, CB15 (Merck)

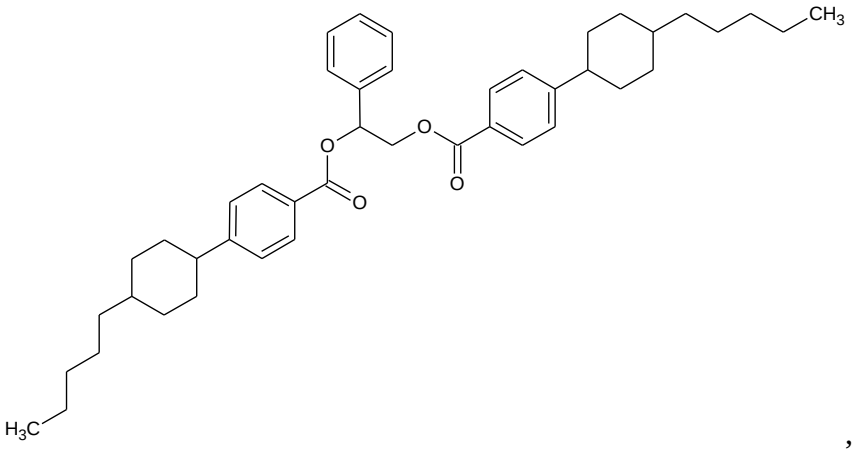

,

ZLI-4572 (Merck)

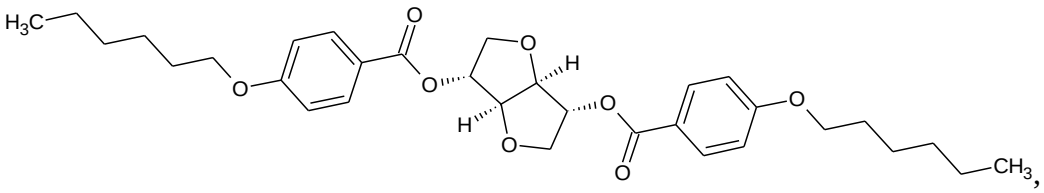

,

ISO-(6OBA)$_2$

Figure 2.2 Molecular structures of three chiral agents.

One of the key parameter to define the characteristic of a chiral agent is the helical twisting power (*HTP*), which is defined as

$$HTP = \frac{1}{P \cdot c}, \tag{2.1}$$

where P is the pitch length, and c is concentration of the chiral agent in the chiral liquid crystal mixture. [5] However, the solubility of chiral agents in nematic liquid crystals depends on the molecular structure. Some material properties of the above mentioned chiral agent is listed in Table 2.2.

Table 2.2 Material parameters of chiral agents.

Parameters	CB15	ZLI-4752	ISO-(6OBA)$_2$
HTP (μm^{-1})*	~7	~50	~50
T_m (˚C)	4	133	80

* HTP is different in different liquid crystal mixture.

2.1.3 Monomers for Liquid Crystal Composites

Besides liquid crystal mixtures and chiral agents, polymer is another critical portion. To chemically build up a polymer composite, monomers are the basic building blocks. Different polymerization approaches, such as heat, light, or electric shocks, can be utilized based on the material properties of the monomers and initiators used in the polymerization process. For simplicity of fabrication, only photolysis is utilized here. Two types of monomers are illustrated in Fig. 2.3.

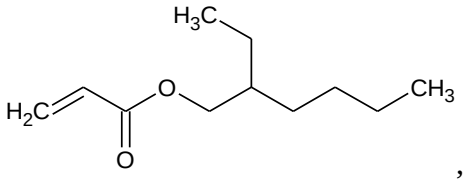

,

EHA (Aldrich)

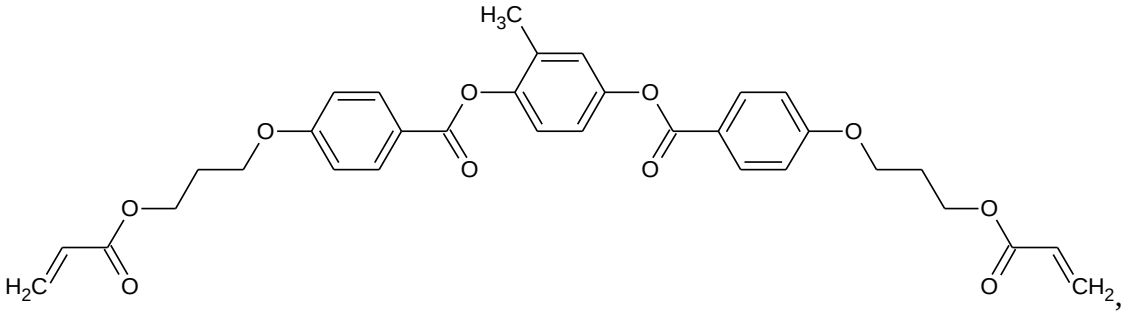

,

RM257 (Merck)

Figure 2.3 Molecular structures of monomers.

As predicted by the molecular structure in Fig. 2.3, distinct material properties would be expected between these two types of monomers. 2-Ethylhexyl acrylate (EHA) is a small molecule monomer. The melting point is -90˚C. RM257 has a larger molecular structure, which indicates a higher melting point. Furthermore, a nematic liquid crystal mesophase is observed in RM257 from 70˚C to 120˚C, which helps the miscibility of this monomer in nematic liquid crystal mixtures. [70]

2.1.4 Supporting Materials

Besides chiral agent doped liquid crystal mixtures, chiral liquid crystal state can also be observed from liquid crystal molecules with chirality by itself. Here we introduce one of the chiral liquid crystal molecules. This chiral liquid crystal molecule itself has a blue phase state with 9-degree temperature range. The molecular structure is presented in Fig. 2.4. [71] Detailed analysis will be discussed as follows.

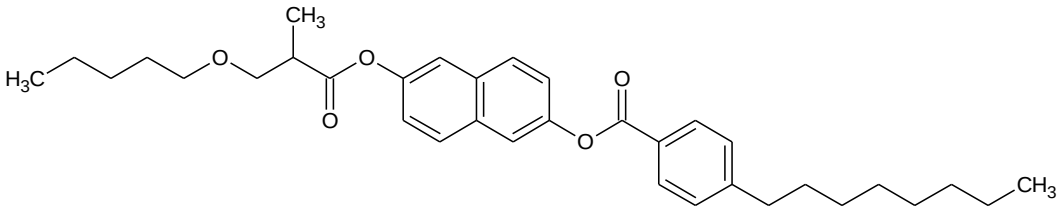

Figure 2.4 Molecular structure of a chiral liquid crystal. [71]

2.2 Characterization Methods

Generally, the mesophase of a chiral liquid crystal mixture can be determined by the phase transition temperature, distinct reflection colors, or electro-optical responses, etc. Here we discuss the above mentioned material systems in the following approaches.

2.2.1 Differential Scanning Calorimetry

Differential scanning calorimetry (DSC) is a thermal analytical technique, in which the difference in the amount of heat required to increase the temperature of a sample and the reference cell is measured as a function of temperature. This method can quantify the amount of heat needed when the sample has a phase transition during heating or cooling cycle.

To find out the transition temperatures between mesophases, DSC is a convenient tool. By several cycles of scanning over a certain temperature range, the transition temperatures can be accurately defined. Fig. 2.5 presents the thermal phase diagram of the chiral liquid crystal compound shown in Fig. 2.4 measured by DSC.

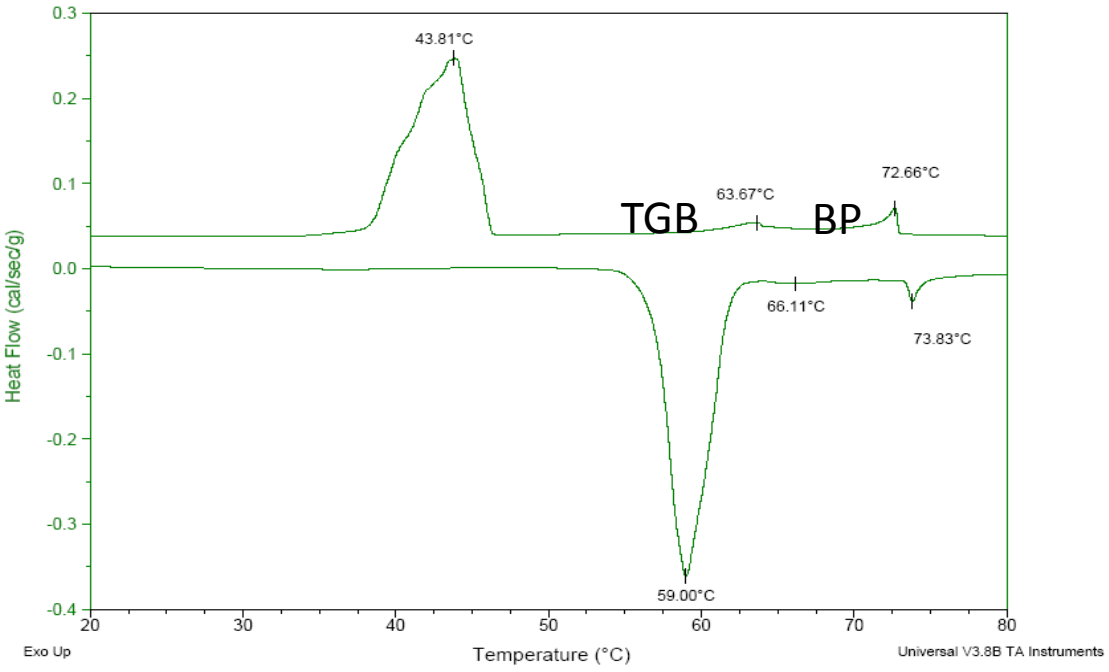

Figure 2.5 DSC measurement of the chiral liquid crystal in Fig. 2.4.

In this material, several mesophases are observed from the DSC diagram. The detail mesophases of this liquid crystal system will be discussed in the following section.

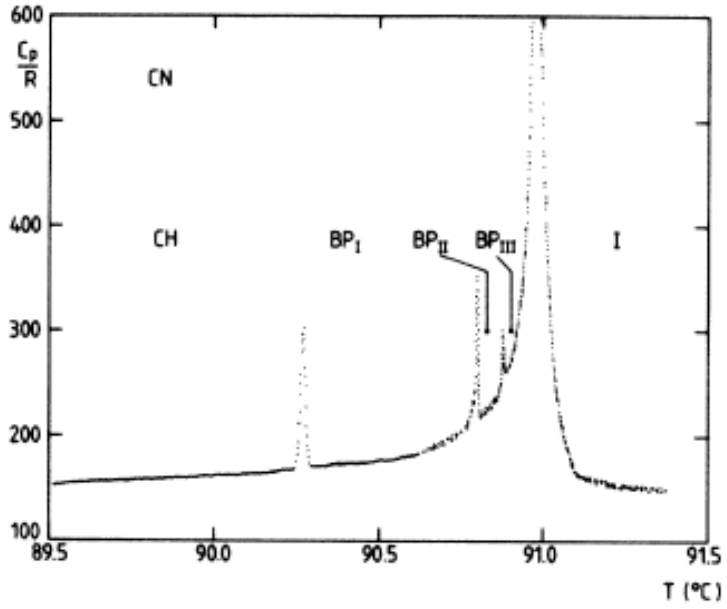

Figure 2.6 Reduced heat capacity in cholesteryl nonanoate. [72] (Reprinted with permission from J. Thoen, *Phys. Rev. A* **37**,1754 (1988) © 1990 by the American Physical Society.)

However, for such a delicate liquid crystal phase like the blue phase state in most of chiral liquid crystal systems, the requirement to the resolution of DSC is very critical. As revealed in Fig. 2.6, the temperature range of each blue phase is very narrow (each blue phase state is less than 0.5˚C) and the heat capacitance is also very small in the cholesteryl nonanoate. [72] The inlet label "CN" stands for cholesteryl nanonate, the "CH" cholesteric liquid crystal state, and the "I" isotropic state. As illustrated in this DSC trace, the heat capacitance (the area under the peaks) between each blue phase transition is very small compared to the heat capacitance in the phase transition to the isotropic state. Additionally, the whole blue phase range, including BPI, BPII, and BPIII, is very narrow, which is less than 1 degree. Because of these reasons, one could easily reach a misleading conclusion that no blue phase state exists if the resolution of a DSC is not enough. Therefore, a high resolution DSC is essential to the identifications of blue phases in different liquid crystal systems.

In this work, the most interesting mesophase to us is the blue phase state. However, limited by the capability of our DSC, most of the BP state in the listed chiral liquid crystal systems cannot be detected. To observe the BP state in these mixtures, we will mainly rely on the next observation approach, polarizing optical microscopy (POM), to investigate the mesophases in our chiral liquid crystal systems.

2.2.2 Polarizing Optical Microscopy

Although it is an exhausting and time-consuming approach compared to DSC, polarizing optical microscopy (POM) is another reliable method to identify the mesophase of a liquid crystal system. The liquid crystal sample in Fig. 2.4 is studied as a comparison between the DSC and the POM approaches. Fig. 2.7 presents the mesophase textures under POM observations at different temperatures.

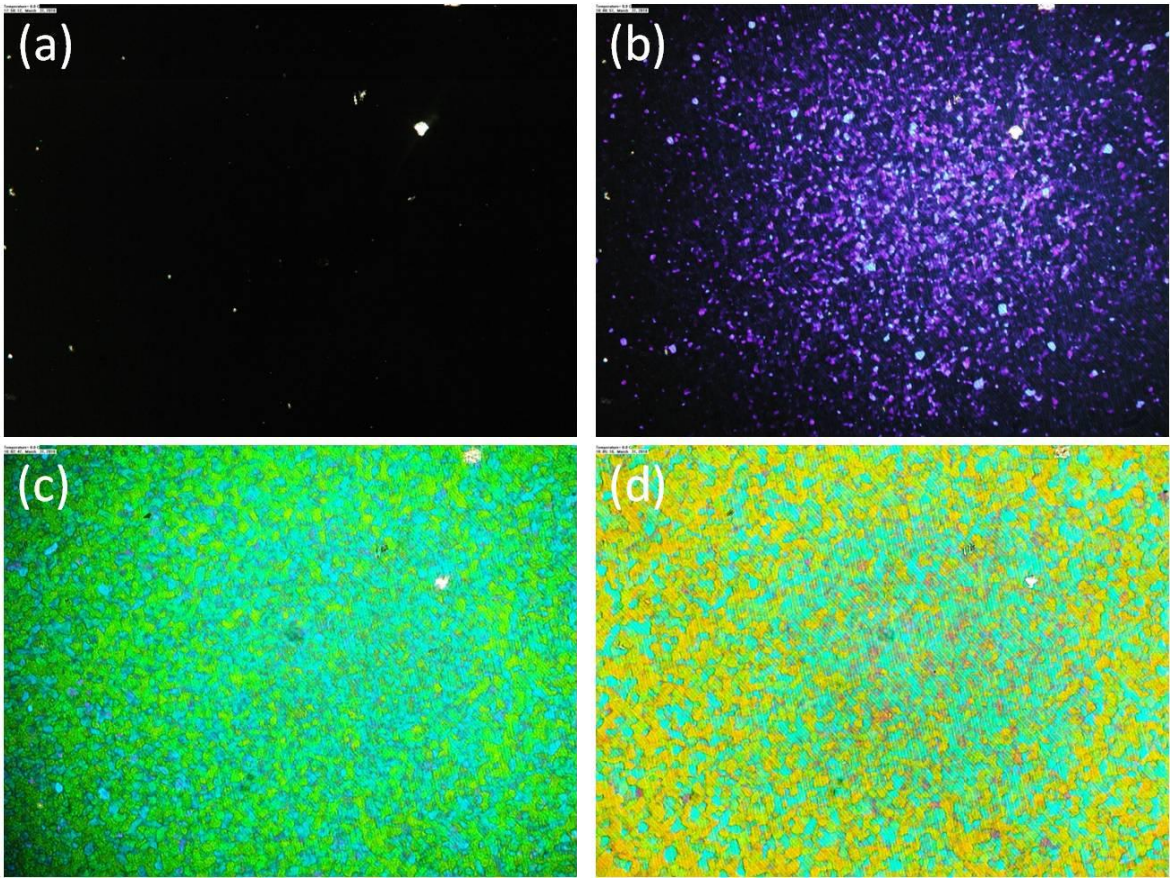

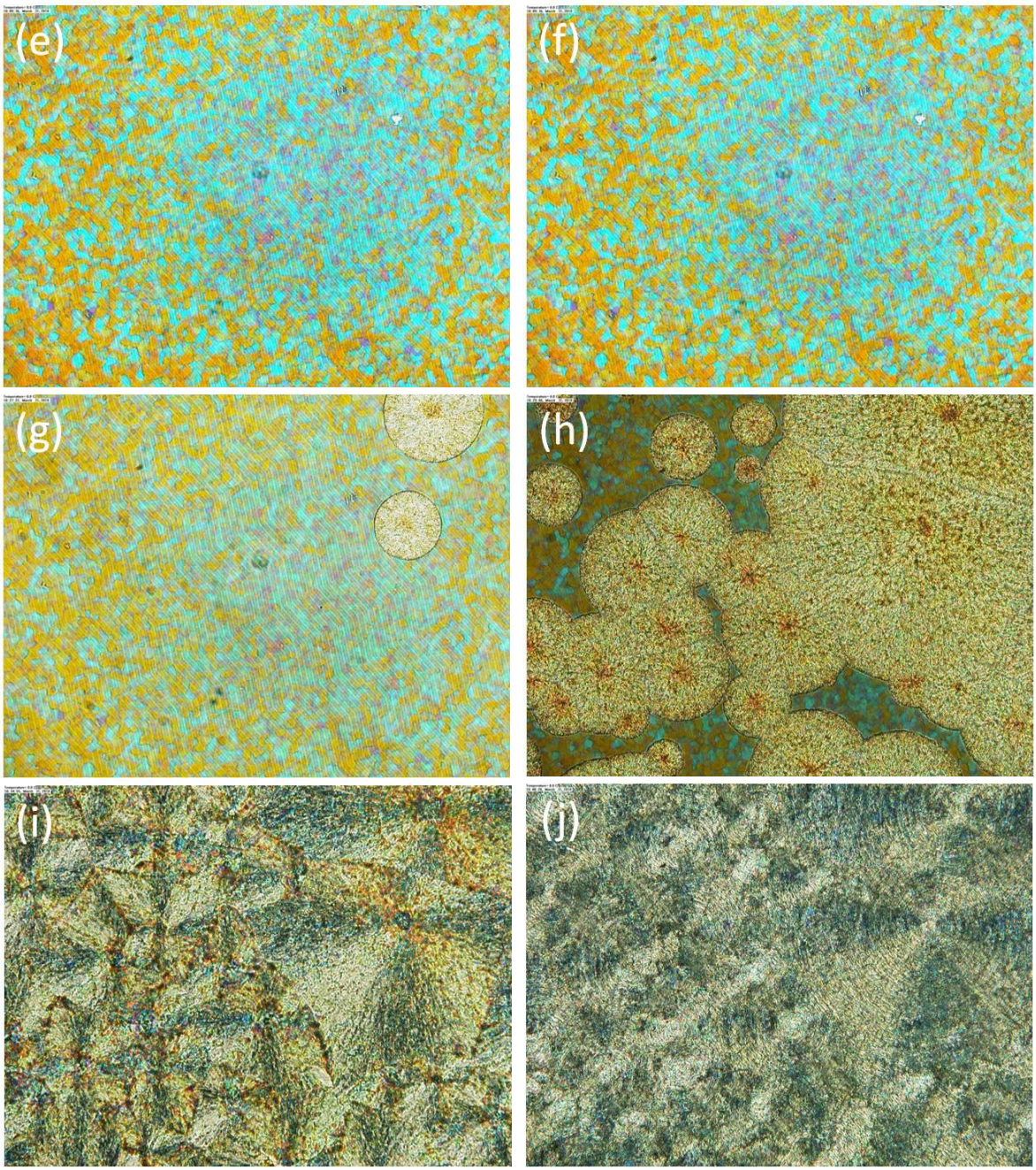

Figure 2.7 POM observations of the liquid crystal molecule in Fig. 2.4 at (a) 75˚C, (b) 73.6˚C, (c) 73.4˚C, (d) 73.1˚C, (e) 73˚C, (f) 72.2˚C, (g) 64.9˚C, (h) 64.4˚C, (i) 63˚C, and (j) 54.4˚C.

As indicated from the DSC phase diagram in Fig. 2.5, the blue phase (BP) state is from 72.6˚C to 63.6˚C and the twist grain boundary (TGB) state shows up below 63.6˚C. The transition temperatures from the DSC measurement are about one degree lower than that from the POM observations. The temperature difference between these two approaches mainly comes from the thickness of the glass substrate used in the POM method, which induces a temperature gradient from the heating stage to the sample. As a result, the BP range of this single molecule system in Fig. 2.7 is about 9 degrees. During the cooling process, within this BP range, the observed color of the BP platelets red-shifts rapidly within one degree and then stays in orange until the TGB phase shows up.

Although a wide blue phase temperature range can be found in this single liquid crystal compound, some other criteria have to be considered while preparing an applicable electro-optical medium for display based on this compound. First of all, the reflection band of a single chiral compound is very difficult to be adjusted. For display applications, the reflection band should be shifted outside the visible range to avoid a colorful reflection. As a result, this compound should be used as a dopant in a proper liquid crystal host. However, the miscibility of this compound is limited as its heat fusion enthalpy is high. Second, the dielectric anisotropy ($\Delta\varepsilon$) of this compound is very small. This small $\Delta\varepsilon$ will lead to a small Kerr constant and, as a result, a high driving voltage. An IPS cell with 5μm electrode width and 10μm electrode space filled with this compound was prepared as a test sample. Though the driving voltage has reached $200V_{rms}$, the transmittance of the sample cell remains quite low under crossed polarizers. Therefore, the criterion of a blue phase liquid crystal system for practical applications would be satisfied easier if the chiral system is prepared by another approach.

The other approach to obtain a chiral liquid crystal system is to add one or more chiral agents into a nematic liquid crystal system. In this work, mixtures prepared by the nematic liquid crystal mixtures in Table 2.1 and chiral agents in Table 2.2 are studied. The compositions of each mixture are listed in Table 2.3.

Table 2.3 Compositions of chiral agent doped liquid crystal systems.

Composition (%)	Mixture-E	Mixture-TL	Mixture-BL	Mixture-TEB
E44	88.5	-	-	-
TL213	-	68.2	-	-
BL038	-	-	70.9	-
TEB300	-	-	-	68.3
ZLI-4752	11.5	6.8	6.7	6.8
CB15	-	25	22.4	24.9

First, we start our searches for BP state from a commonly used E-series liquid crystal mixture, E44. As discussed, to induce BP state, high chirality in a chiral liquid crystal system is preferred. [16] However, each chiral agent has different limit of miscibility in different liquid crystal mixture. In Mixture-E, although 11.5% of ZLI-4752 was added, blue phase state was still not observed. Increasing the concentration of ZLI-4752 would solidify the mixture during the cooling process. Therefore, Mixture-TL (based on TL213) was investigated as the second sample. After mixing the designated ratios well, BP state was observed from 49.1˚C to 47.2˚C under POM during the cooling process. Fig. 2.8 shows the POM observations over the whole BP range. The BP phase range in Mixture-TL is from 49.1˚C to 47.2˚C, which is only 2 degrees.

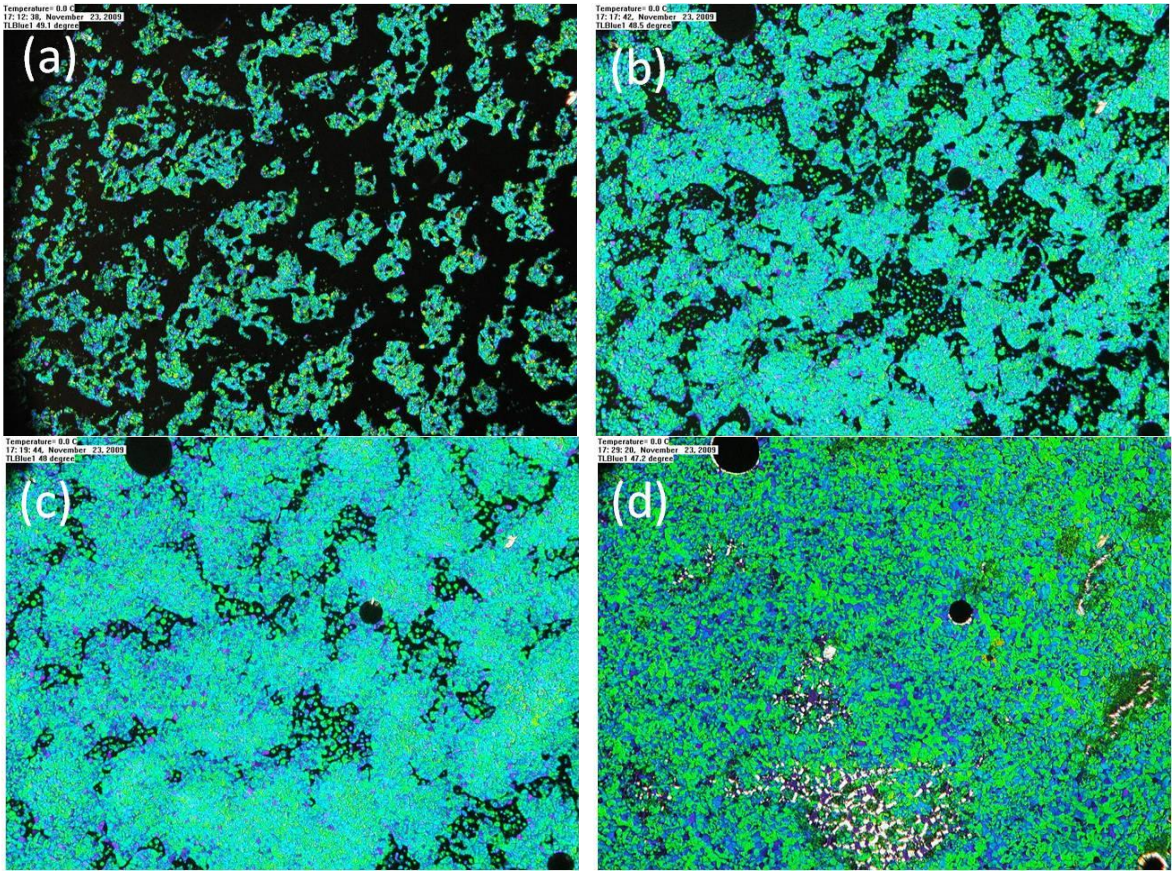

Figure 2.8 POM observations of Mixture-TL at (a) 49.1˚C, (b) 48.5˚C, (c) 48˚C, and (d) 47.2˚C.

The third mixture is based on BL-series nematic liquid crystal, BL038. Fig. 2.9 shows the POM pictures of the BP state in Mixture-BL. The BP state range is from 69.5˚C to 66.5˚C, where the BP state is about 3-degree wide.

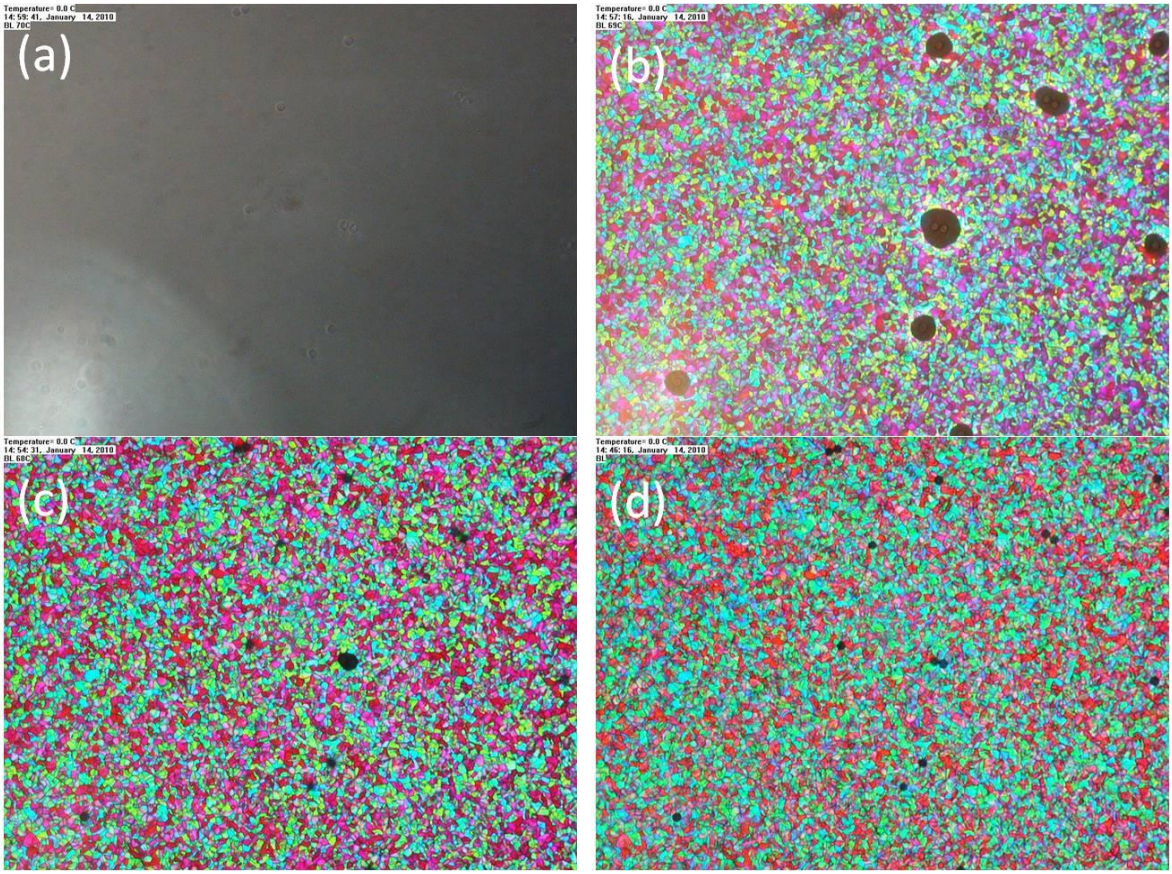

Figure 2.9 POM observations of Mixture-BL at (a) 70˚C, (b) 69˚C, (c) 68˚C, and (d) 66.5˚C.

The last mixture, Mixture-TEB, is based on a nematic liquid crystal mixture, TEB300. The observed BP state is about 3-degree wide; from 33˚C to 30˚C during the cooling procedure. The POM pictures are presented in Fig. 2.10 at different temperatures.

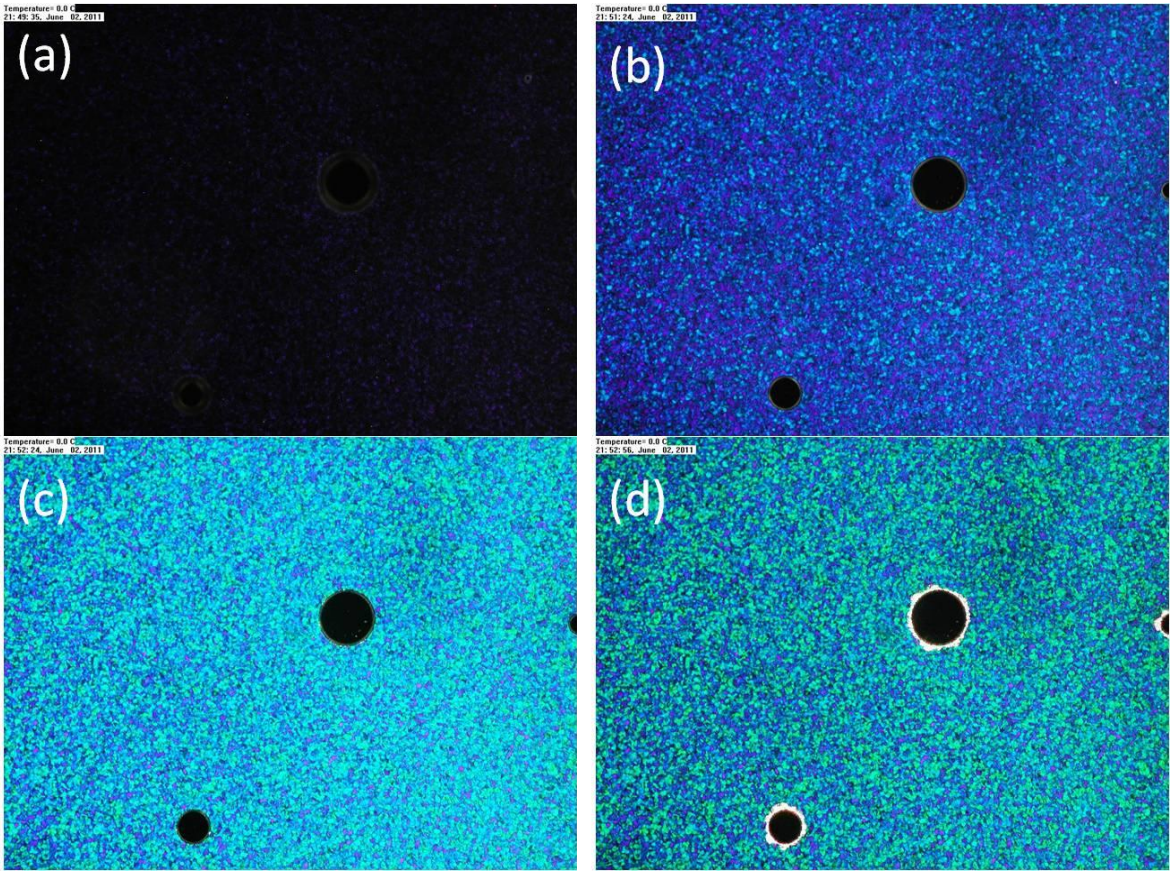

Figure 2.10 POM observations of Mixture-TEB at (a) 33˚C, (b) 31.5˚C, (c) 30.4˚C, and (d) 30˚C.

As presented from Fig. 2.8 to Fig. 2.10, though two same types and a comparable weight ratio of the chiral agents were added, the color of the BP platelets, which indicates the induced chirality, was different in different nematic liquid crystal hosts. Moreover, the temperature range of the BP states is located at a different level and has a different width. A narrow BP range (e.g., Mixture-TL) and a low temperature level in Mixture-TEB make the LCD panel fabrication and characterization much more difficult.

2.2.3 Electro-Optical Responses

Electro-optic (EO) response is another approach to identify the mesophases of a liquid crystal system. Similar to the case that various EO responses could be distinguished between different mesophases, like ferroelectric, sematic, or nematic phases, based on a similar or even the same system compositions. BP liquid crystal system also possesses this feature between different BP states. According to U. Singh, the induced refractive index in each BP phase is different. [73] Fig. 2.11 shows the electric field-induced birefringence from BP to the isotropic states based on cholestryl nonanoate.

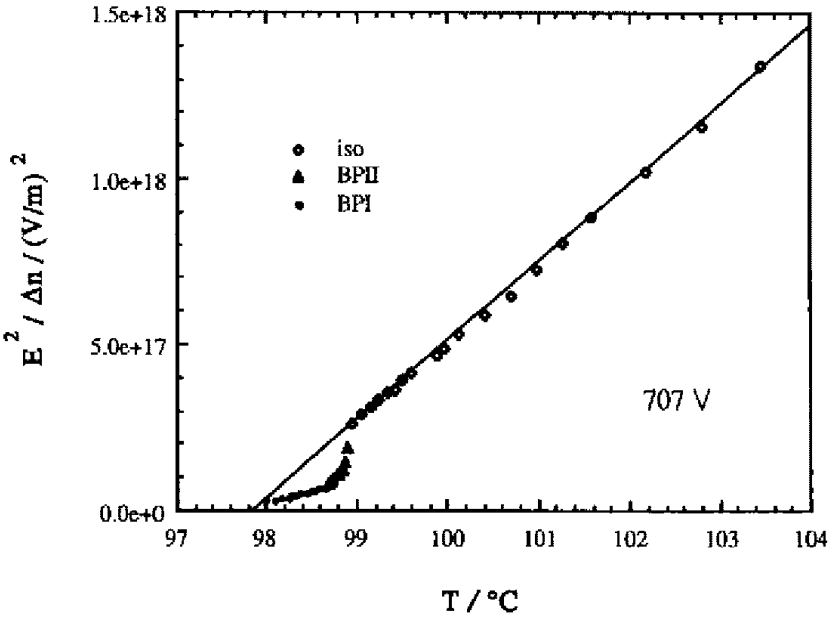

Figure 2.11 $E^2/\Delta n$ versus temperature for cholestryl nonanoate at an applied voltage of 707V. [73] (Reprinted by permission from Taylor & Francis: Liquid Crystals, © 1990)

As indicated in Fig. 2.11, the electric field induced birefringence in BPI state is higher than it in BPII or isotropic phase. Based on this feature, we can roughly identify the BP states of

a chiral liquid crystal system. Further details on one of the listed chiral liquid crystal mixtures will be discussed in the following chapters.

2.3 Summary

To prepare a viable blue phase mixture, multiple factors should be considered, for example, the capability of having a BP state as wide as possible at a reasonable level of temperature, the miscibility of components in the system, the stability of the entire system, and an acceptable operating voltage. Therefore, to prepare a BP liquid crystal mixture, the material properties of individual composition have to be carefully considered. After all components are mixed homogeneously, the properties of the whole system also have to be checked again. From the above characterization methods to the mixtures in Table 2.3, the BP state was not observed in Mixture-E. As for Mixture-TL, the temperature range is too narrow, which will lead to difficulties in sample preparation and characterization. Moreover, though a relatively wide BP range is found in Mixture-TEB, it shows up at room temperature, which is too sensitive to the environmental conditions. Based on the above considerations, Mixture-BL is used for further sample preparations and characterizations of the BP properties.

CHAPTER 3: BLUE PHASE LIQUID CRYSTALS

Although liquid crystal molecule with an intrinsic chirality could be a candidate for forming blue phases, chiral agent doped-nematic is still preferred because of its simple control of chirality. After considerations over blue phase liquid crystal mixtures from different series of liquid crystal hosts discussed in chapter 2, Merck BL series is a promising LC host for further studies.

3.1 Material System

For transmissive displays, BP reflection band in the visible range should be avoided. By adjusting the concentration of chiral agents, the reflection band of a BP mixture could be pushed into either ultraviolet (UV) or infrared (IR) region. However, based on prior discussions, [16] it is easier to induce a BP state in a high chirality system than it is in a low chirality system. As a result, mixture UVBL based on Merck BL LC host was prepared by modifying the ratio of the chiral agents up to 25%.

3.2 Thermal Morphology

Thermal morphology is an important parameter as the commencement of the total evaluations. Both DSC and POM approaches were used here.

3.2.1 Differential Scanning Calorimetry Results

First, we used DSC to measure the thermal features of mixture UVBL and results are presented in Fig. 3.1.

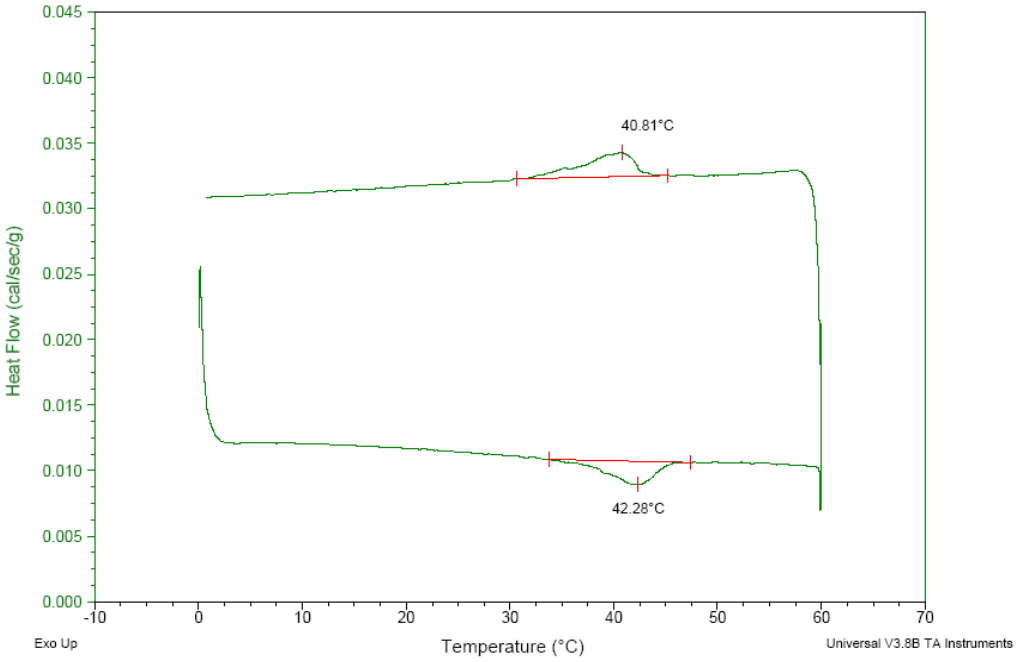

Figure 3.1 DSC diagram of mixture UVBL.

As shown, between 60˚C to 0˚C only one broad bump of heat flow around 40˚C was detected. From this DSC result, it is difficult to identify which type of mesophase exists in mixture UVBL. Therefore, another characterization method, the POM approach, was performed.

3.2.2 Liquid Crystal Texture

As the mesophase cannot be identified via DSC, POM observation becomes the important key to find the thermal morphology. After searching the entire span of temperature as shown in DSC, the observed POM pictures are presented in Fig. 3.2.

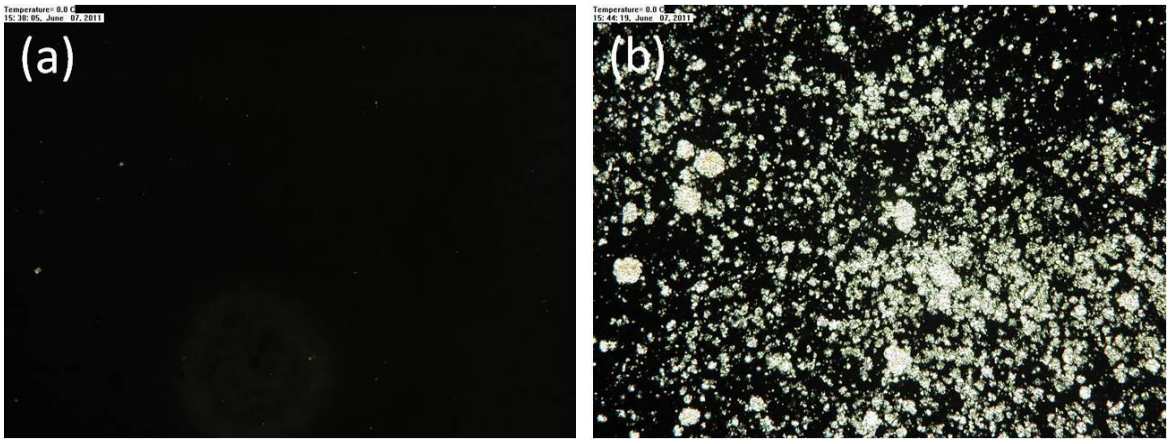

Figure 3.2 POM observations of mixture UVBL at (a) 41.5˚C, and (b) 36.5˚C.

As shown in Fig. 3.2, the observed POM is colorless and completely dark. To confirm a BP state from POM observations, BP platelets would be the direct evidence to it. However, no color reflection should be expected under POM observations since the BP reflection band of mixture UVBL was shifted to UV region for display application. Fortunately, though invisible in the visible region, slight light leakage, because of the orientation of BP platelets, could help in the confirmation of the BP state. By enhancing the contrast ratio and the brightness with post image processing, BP platelets can be observed as shown in Fig. 3.3. [38]

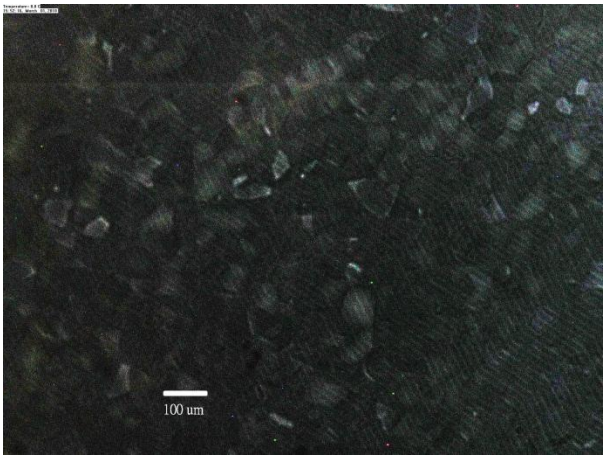

Figure 3.3 The enhanced image of BP platelets in mixture UVBL. [38]

As a result, BP state can be confirmed in mixture UVBL which is from 41.5˚C to 36.5˚C and 5-degree wide. After further examinations over the whole BP range, two BP states, BPII and BPI, were found above and below 39.3˚C accordingly. The EO performance in different BP states will be discussed next.

3.3 Electro-Optics of Blue Phase Liquid Crystal

Besides thermal morphology, EO response in BPLC is another important issue for practical display applications. Because of the crystalline-like molecular arrangement, the EO characteristic is rather complicated in the BP states. [74] Various electric field-induced phenomena were described from early works until now. [75] [74] Conceptually speaking, as the electric field increases the double helix structure in BPLC unwound gradually to different liquid crystal states as illustrated in Fig. 3.4. [76] [77]

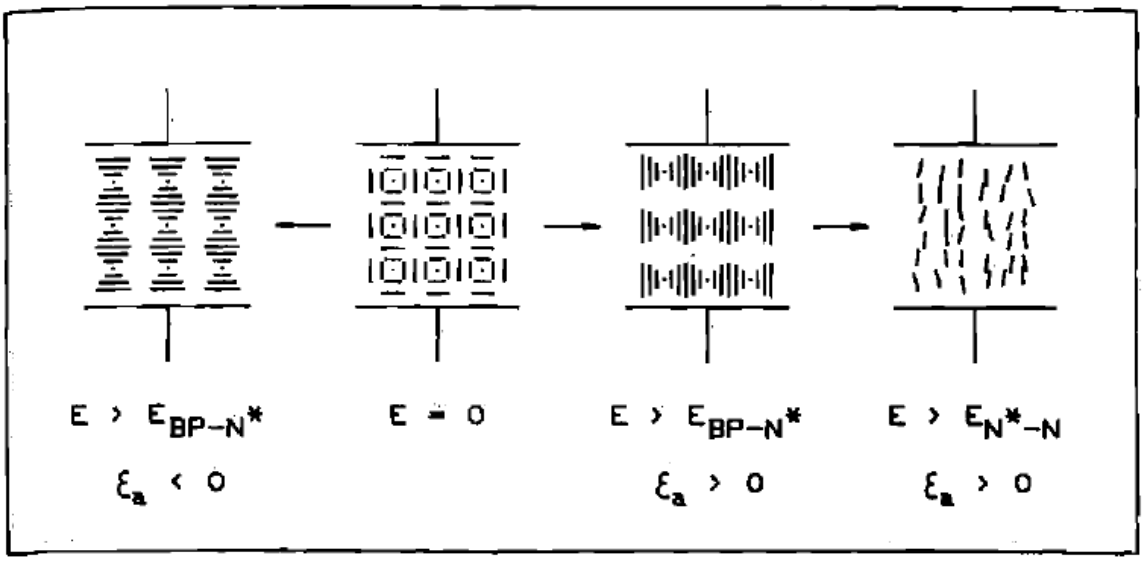

Figure 3.4 Electric-field-induced unwinding scheme in BPLC. [76] [76]

(Reprinted by permission from Taylor & Francis: Molecular Crystals and Liquid Crystals, © 1991)

Further studies indicate that the electric field-induced effects in a BPLC system can be categorized into three types, i.e., local molecular reorientation, electrostriction, and phase transition. [76]-[86] First of all, the mechanism of local molecular reorientation is as depicted as its name. Under an electric field influence, only the LC molecular orientations aligned either parallel or perpendicular to the direction of the electric field is involved. Usually, the response time of this mechanism is at the level of hundreds of microseconds. The second mechanism is electrostriction. In this level of operation, the macroscopic molecular arrangement, i.e., the lattice structure in BPLC system will be either compressed or stretched depending on the direction of the electric field, the orientation of the BPLC lattice facets, and the physical properties of the BPLC molecule. Fig. 3.5 illustrates the deformations of two BPLC systems with (a) positive and (b) negative dielectric anisotropy at different lattice orientations under the same electric field direction, respectively.

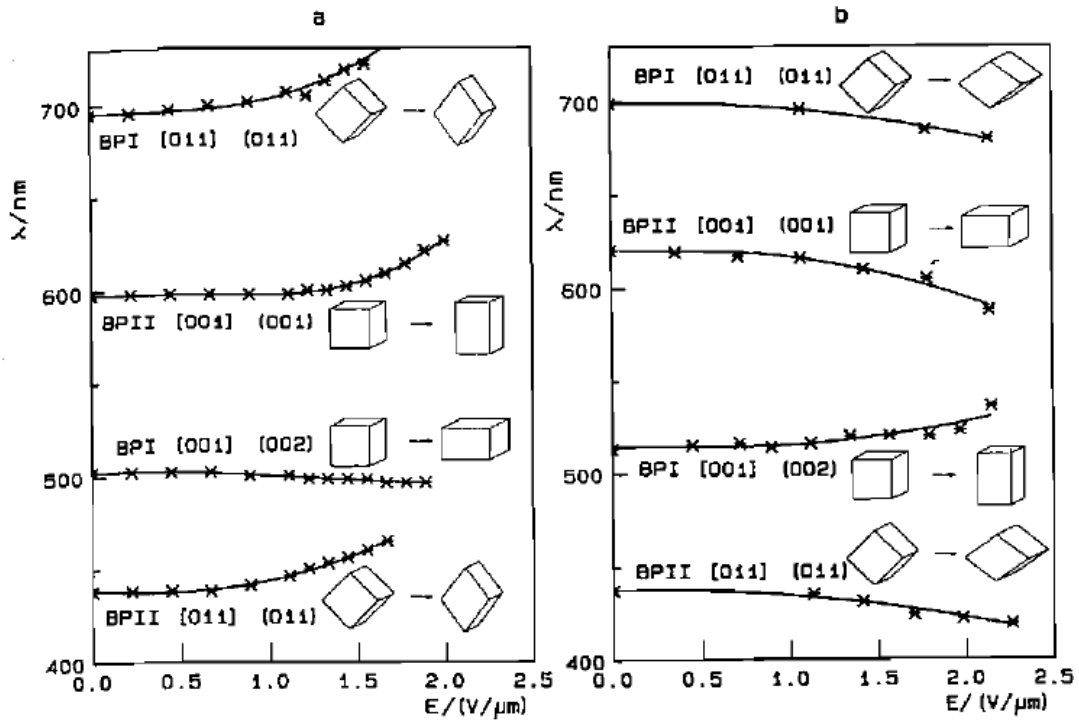

Figure 3.5 Electrostriction in BPLC. [77] [84] [85] (Reprinted by permission from Taylor & Francis: Molecular Crystals and Liquid Crystals, © 1991)

With this electric field-induced deformation, the reflection wavelength shifts in order to satisfy the required Bragg condition. Usually, the response time of this mechanism is at a level of tens of milliseconds. The last electric field-induced mechanism is phase transition. Because of the perturbation from the external electric field, the stacking of BPLC molecules changes according to a locally stable free energy state. As a result, various possible electric field-induced stable BPLC states can be observed. Fig. 3.6 presents some phase transition schemes under an external electric field influence. [77]

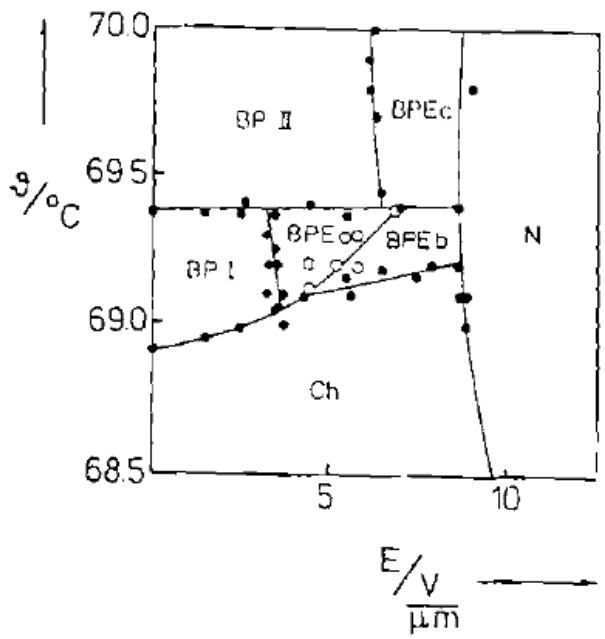

Figure 3.6 Electric field induced phase transitions in BPLC. [77] (Reprinted by permission from Taylor & Francis: Molecular Crystals and Liquid Crystals, © 1991)

Usually, the response time of phase transition is very slow which is about hundreds of milliseconds. In some cases, this phase transition feature even takes hours.

Macroscopically speaking, BPLC is optically isotropic at the field-off state. When an electric field is present, it shows different induced birefringence depending on which orientation of the crystalline structure is aligned to the electric field direction. [75] [77] [86] In a BP molecular structure with cubic symmetry, the Kerr effect is described by three independent electro-optic coefficients. [87] However, if biaxiality is neglected and if the average refractive index is assumed to remain constant, the field-induced refractive index can be regarded as the Kerr effect in an isotropic liquid. [75] Therefore, it can be approximately described by a single

Kerr coefficient [88]

$$K = \frac{\Delta n}{\lambda E^2}, \tag{3.1}$$

where Δn is the electric field induced birefringence, λ is the wavelength of the incident light, and E is the electric field. Therefore, in a simplified scenario, the approximated electric field-induced birefringence occurs only in the electric field affected region and also alone the same direction of the electric field. As a result, to effectively introduce phase retardation to the incident light, the electric field should be perpendicular to the propagation direction of the incident light. Therefore, IPS (in-plane-switching) electrode geometry would be a proper structure to fabricate a BPLC cell.

In this chapter, a BPLC sample is prepared by filling mixture UVBL into an empty glass cell. The top substrate is a piece of plain glass. As for the bottom glass substrate, a thin layer of interdigitated transparent ITO (indium-tin-oxide) electrodes in IPS geometry is coated. The cell gap of sample UVBL is controlled at ~13 μm by spacer balls. Because the molecular arrangement in BP state is formed by self-assembly process, rubbing process is not required. Furthermore, because of the IPS electrode geometry, the EO performance of a BP sample is not sensitive to the cell gap when it is larger than a certain thickness. [48]

To measure EO responses, a He-Ne laser (λ=633 nm) was used as the light source. Sample UVBL was placed between two crossed polarizers. Ideally, when the electric field is uniform the transmittance (normalized to that of two parallel polarizers) of the BPLC cell through crossed polarizers can be described by following equation [89]

$$T_{\perp} = \sin^2(2\phi)\sin^2\left(\frac{\delta}{2}\right), \tag{3.2}$$

where ϕ is the angle of the polarization of the incident light with respect to the front polarizer, and δ is the electric-field-induced phase retardation from the test sample. When the polarization direction of the incident light is at 45° to the polarizer (i.e., ϕ=45°), the transmittance in equation (3.2) is only related to the phase retardation of the sample. Therefore, a maximum transmittance can be detected when phase retardation (δ) of the test sample matches integers of π. In an IPS electrode geometry, the phase retardation δ in a BP sample can be roughly approximated as

$$\delta = \frac{2\pi}{\lambda}\Delta n d = 2\pi K E^2 d \,, \tag{3.3}$$

where K is the Kerr constant, and d is the effective thickness of the induced birefringence layer. With this electric field-induced phase retardation, the transmitted light intensity can be modulated by the applied voltage signal. Therefore, the static EO response (the voltage induced transmittance curve, VT) can be recorded as the reference for further gray level operations.

The driving electric signal here is composed of a 1 kHz square wave signal of 50% duty cycle. To confirm the stability of this sample, two or more cycles of voltage ascending and descending procedures were consecutively executed during the measurement. As found in section 3.2, there are two BP states in mixture UVBL. Therefore, the EO characteristics in these two BP states will be discussed respectively in this section.

3.3.1 Blue Phase I

First of all, the voltage-dependent transmittance (VT) of sample UVBL at BPI state was measured as Fig. 3.7 shows. Two cycles of voltage ascending and descending procedures were performed.

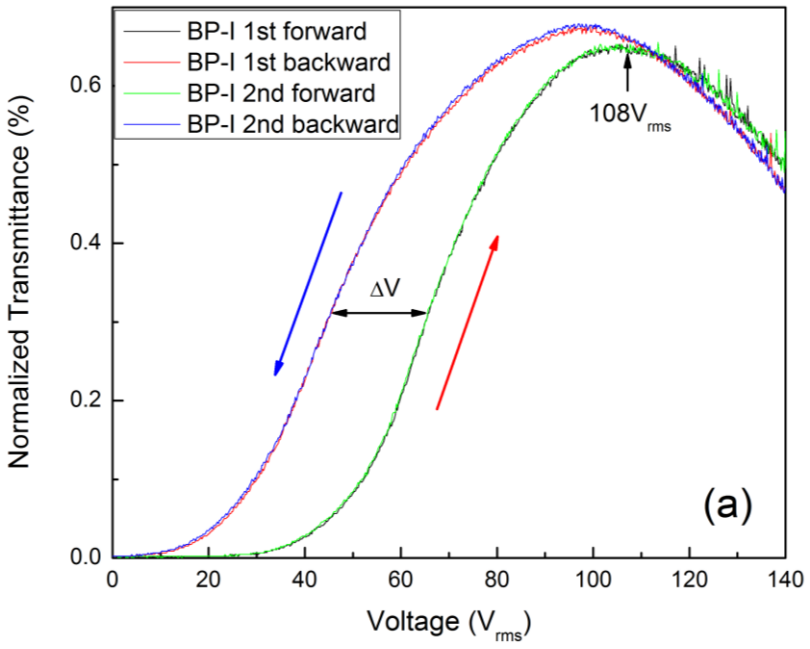

Figure 3.7 Measured VT curves of sample UVBL at BPI state (λ=633nm).

As mentioned in section 3.1, the reflection band of sample UVBL is shifted to the UV region for display applications. Moreover, because of the intrinsic optically isotropic property at the voltage-off state, the setup of sample UVBL between two crossed polarizers is a normally black device, i.e., no light is transmitted through the analyzer at V=0. The transmittance of the dark state basically depends only on the extinction ratio of the polarizer. Therefore, the initial transmittance in Fig. 3.7 is very low. As voltage increases, the induced phase retardation accumulates accordingly by equation (3.3). As a result, the detected transmittance through sample UVBL increases along the lower curve which is labeled by a red arrow in Fig. 3.7. When voltage rises up to ~108V_{rms}, the transmittance reaches a maximum. After this maximum, transmittance decreases because of an excessive phase retardation induced by a higher voltage.

As in the procedure during voltage descending, the detected VT curve rises up first, because of the decreasing of phase retardation, and then reduced back to its initial low

transmittance dark state along the higher curve which is labeled by a blue arrow in Fig. 3.7. Here, a voltage difference (ΔV) is observed between the ascending and the descending VT curves at half transmittance level. This observed phenomenon is called "hysteresis". Generally, the quantity of hysteresis can be defined as

$$Hys = \frac{\Delta V}{V_p}, \tag{3.3}$$

where V_p is the peak transmittance voltage.

Hysteresis is a well-known phenomenon in electronic, magnetic, and optical systems. [90] [91] Generally speaking, hysteresis should be less than 1% in order to obtain accurate gray-scale control. Here, the calculated hysteresis of the VT curves in Fig. 3.7 is 18.5%.

Dynamic EO response, i.e., the response time, is another critical performance evaluating factor in liquid crystal devices. Fig. 3.8 presents the dynamic response time from sample UVBL between crossed polarizers.

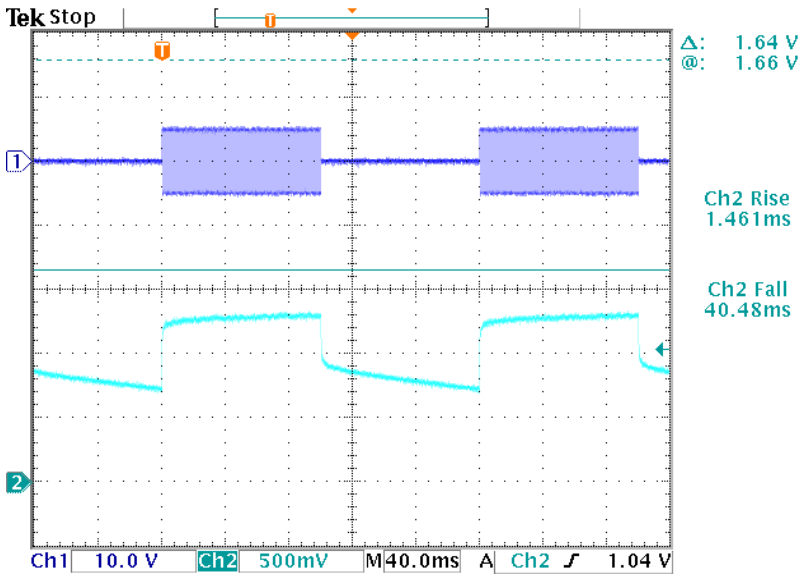

Figure 3.8 Full on-off response time of sample UVBL at BPI state.

The driving pulse signal here is composed of series of square waves in 1 kHz with 50% duty cycles in two voltage states. The on-state voltage is set at the peak transmittance voltage in Fig. 3.7 and the off-state voltage is at 0V. As shown in Fig. 3.8, the upper trace is the driving voltage waveforms while the lower trace is the detected optical signals through the whole setup. From the optical response curve, the rise time of sample UVBL is ~1.5ms and the fall time is ~40.5ms. As illustrated in the optical response trace, two relaxation slopes involved in the voltage on-off transitions could be distinguished. It can be clearly observed from the switch-off transition that one relaxation process is in the submillisecond level; while the other is in tens of milliseconds. Furthermore, during the relaxation transition the transmitted light intensity does not go back to its initial dark state within the given relaxation time. This indicates the required recovery time should be more than 100ms or a deteriorated dark state will be observed. Based on above observations, at least two mechanisms are involved in the EO process. Comparing from the relaxation time scales, local molecular reorientation and electrostriction should be the two main mechanisms in this driving scheme. Phase transition might be also involved in the EO transition. However, the short period of the pulse driving signal makes it unable to be confirmed.

3.3.2 Blue Phase II

According to the thermal scheme in section 3.2, another blue phase state, BPII, was observed in mixture UVBL when the temperature was above 39.3˚C. Based on the molecular stacking geometry in Fig. 1.8, the lattice structure is different in each BP state. Therefore, different EO properties could be expected when sample UVBL was operated above 39.3˚C in the BPII state.

Fig. 3.9 shows the VT curves from sample UVBL in BPII state with two voltage scanning

cycles. As discussed before, the transmittance increases with an increasing voltage. When the driving voltage is increased to 143V_{rms}, maximum transmittance was reached. Comparing to the maximum transmittance voltage ~108V_{rms} at BPI state, the peak transmittance voltage is higher in BPII state. This is because of a smaller Kerr constant in BPII state. [73] During the voltage descending procedure, the decreasing transmittance overlaps the same trace from the ascending procedure. As a result, different from operating sample UVBL in BPI state, no hysteresis was observed when sample UVBL was operated in BPII state.

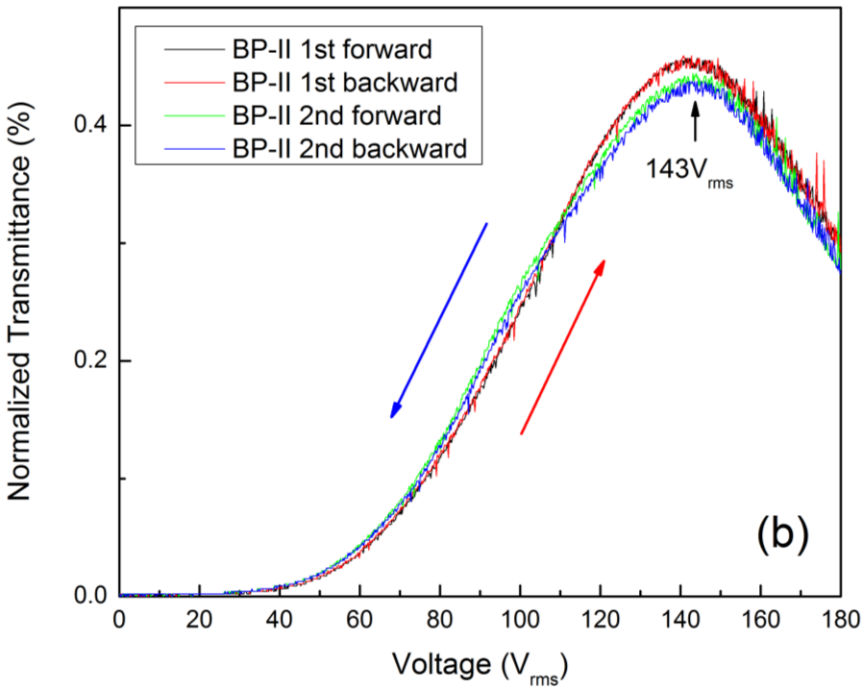

Figure 3.9 Measured VT curves of sample UVBL at BPII state (λ=633nm).

Besides the difference in static EO responses, the dynamic response between BPI and BPII is also quite different. Fig. 3.10 shows the full on-off response time of sample UVBL at BPII state.

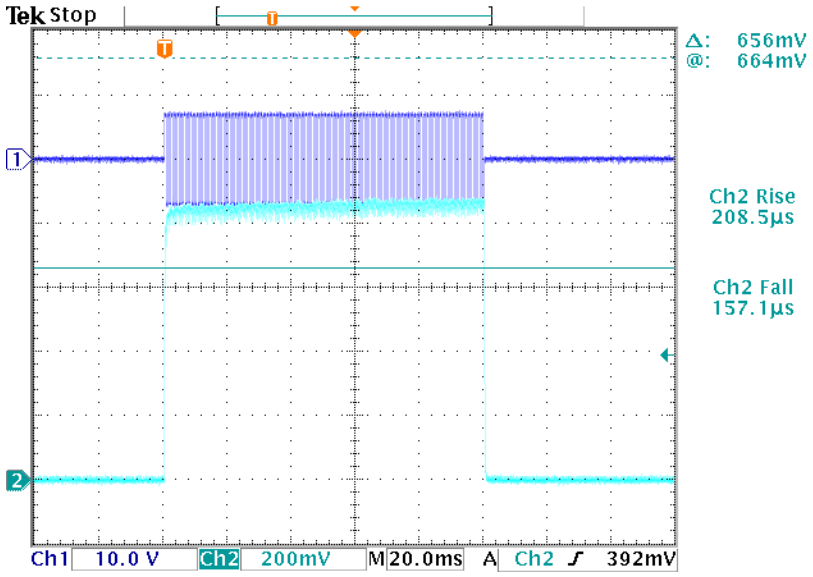

Figure 3.10 Full on-off response time of sample UVBL at BPII state.

Same operation scheme in Fig. 3.8 was applied in Fig. 3.10. By switching the driving voltage between 0V and 143V_{rms}, the measured rise time is 208.5µs and the measured fall time is 157.1µs. Comparing to the response time in BPI state shown in Fig. 3.8, only one relaxation process was observed in the BPII state and the response time was reduced dramatically to the submillisecond level.

Until now, various methods starting from different perspectives are used to describe the expression for the dynamic behavior in BPLC. [16] Kitzerow et al, uses Dmitrienko's free energy density equation [92] to describe an initially cubic blue phase lattice in a field E [79]

$$F = \frac{1}{2}\Lambda\left[\frac{du}{dx}\right]^2 - \frac{1}{8\pi}pE^2\left[\frac{du}{dx}\right] - \frac{1}{16\pi}\chi E^4, \tag{3.4}$$

where u is the lattice displacement, Λ the elastic related constant, p the elasto-optic coefficient, χ the nonlinear dielectric susceptibility, and electric field E is assumed to be in x direction only.

After applying the assumptions of unconstrained boundary, incompressible and rest background fluid, the relaxation time constant can be expressed as

$$\tau \sim \frac{\gamma_1}{K_2 q^2}, \tag{3.5}$$

where γ_1 is the twist viscosity, K_2 the twist elastic constant, and $q=\pi/p$, the inverse of the pitch length.

Another perspective described by Glesson et al [83] is to analogously use the field induced unwinding mechanism in the cholesteric (single axis helical structure) state. They assumed that the same process happened in the BP (double axes helical structure) state based on Jakeman and Raynes' works [93]. Under the assumptions of negligible bulk fluid motion and small rotation angle, the time varied rotation angle ϕ between the director and the applied field is expressed as

$$\frac{\partial \phi}{\partial t} = \frac{1}{\gamma_1}\left\{\frac{\Delta \varepsilon E^2}{4\pi} + K_2 \frac{\partial^2}{\partial x^2}\right\}\phi. \tag{3.6}$$

From equation (3.6), the rise and fall time is given by

$$\tau_{fall} = \frac{\gamma_1}{K_2 q^2}, \tag{3.7}$$

$$\tau_{rise} = \frac{\gamma_1}{\frac{\varepsilon_0 \Delta \varepsilon E^2}{4\pi} - K_2 q^2}. \tag{3.8}$$

As presented above, the response time equations from different perspectives lead to the same expression. In our sample UVBL, the pitch length of sample UVBL is about 200nm which

can be calculated from the peak wavelength of the reflection band. By plugging in the required parameters, the estimated fall time from equation (3.7) is about 0.15ms, which matches the scale of the measured decay time in Fig. 3.10. This measured full on-off response time also agrees well to those published previously by other groups. [28] [79] [82] [83] Another interesting comparison between sample UVBL and the conventional liquid crystal devices is that the response time in BPII state is about one order faster and below 1ms.

The expressions of the response time in the blue phase state in equations (3.7) and (3.8) are similar to those of nematic liquid crystals as presented in the following equations

$$\tau_{fall} = \frac{\gamma_1 d^2}{K_{11}\pi^2}, \tag{3.9}$$

$$\tau_{rise} = \frac{\gamma_1}{\varepsilon_0 \Delta\varepsilon E^2 - \frac{K_{11}\pi^2}{d^2}}, \tag{3.10}$$

where γ_1 is the rotation viscosity, K_{11} the splay elastic constant, and d the cell gap.

From above equations, an extreme case could be assumed as follows. When the pitch length (p) of a chiral liquid crystal system, for example the blue phase state, becomes infinitely long, the pitch length could be treated as the cell gap (d). Therefore, in this case, this infinite pitch length blue phase liquid crystal system can be regarded as a nematic liquid crystal system. As a result, the response time expressions in equations (3.7) and (3.8) can be approximated to equations (3.9) and (3.10). Generally speaking, the thickness of a nematic liquid crystal cell is about 4μm. Thus, calculated from equations (3.9) and (3.10), the response time in a nematic liquid crystal cell is about tens of milliseconds.

3.4 Summary

In chapter 3, a potential BPLC system for display applications is evaluated in the thermal morphology and the EO responses. Based on the thermal properties of UVBL system, two BP states, BPI and BPII, are observed. The EO responses in these two BP states are also characterized respectively. According to the experimental observations, each BP state possesses its own distinct EO responses. When the sample UVBL is operated in the BPI state, the peak voltage corresponding to the maximum transmittance is lower because its Kerr constant is larger. However, the total response time in the BPI state is at the level of tens of milliseconds due to different field induced mechanisms involved. Also, the hysteresis problem is severe when sample UVBL is operated in the BPI state. As for the EO responses in the BPII state, though the peak voltage is higher compared to that in BPI, the response time in the BPII state is about 2 orders faster than it in the BPI state and the no hysteresis problem is observed.

However, for real applications the thermal stability is one of the major issues in BPLC systems. As discussed in the above sections, the BP temperature range in this system is very narrow (only 5 degrees). This narrow temperature range greatly limits the usefulness of this BPLC system in practical applications. To overcome this limited BP range, several temperature range widening approaches are described. In next chapter, we will discuss the polymer stabilization approach for our UVBL mixture.

CHAPTER 4: POLYMER-STABILIZED BLUE PHASE LIQUID CRYSTALS

Limited by its narrow temperature range, although possessing many attractive properties blue phase liquid crystal does not prevail in the past three decades. Until recently, many approaches have been proposed to overcome this obstacle, such as molecular engineering [24] [25], mixture doping or combinations [26] [27], etc. In 2002, Kikuchi et al proposed polymer stabilization method to expand the stable blue phase range from 1 degree to over 60 degrees. [28] In 2005, Coles et al demonstrated a symmetric molecule structure to achieve a wide blue phase range over 40 degrees. [24] In this chapter, with the considerations of further EO properties and system feasibility, we utilized the photo-induced polymer stabilization approach based on mixture UVBL to obtain a wide temperature polymer-stabilized blue phase liquid crystal (PS-BPLC) sample.

4.1 Material System

To prepare a photo-induced polymer precursor, the UVBL system was further doped with the monomers in section 2.1. Also, in order to have an easy processing system which possesses a proper EO response, ester liquid crystal compound, C3PEstP(3F)EstP(3F)CN, was added to the UVBL system. The molecular structure of the compound is presented in Fig. 4.1.

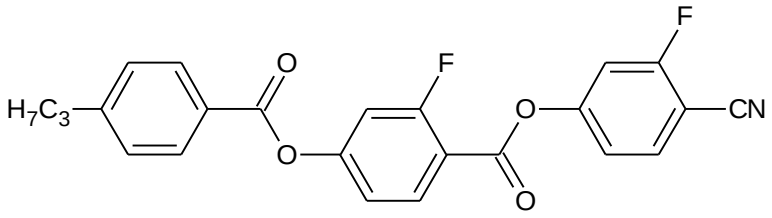

Figure 4.1 Molecular structure of C3PEstP(3F)EstP(3F)CN.

The dielectric anisotropy of this ester compound is about 60. [94] The amount of this compound was added as high as possible to increase the dielectric anisotropy of the whole system while keeping the mixture mixed homogeneously. Because of the dramatic difference between the physical properties of each required components, the ratio of each component has to be carefully adjusted and optimized in order to obtain the blue phase state. Moreover, to stabilize a blue phase material over a wide temperature, the ratio of monomers is also very critical. [95]

4.2 Textures and Phase Morphologies

To evaluate the impacts of the polymerization conditions, two polymer precursors, VIS-PSBP and UV-PSBP, were prepared. For evaluation simplicity, the reflective color of the VIS-PSBP mixture was adjusted to the green color. While in the UV-PSBP, the reflection band was shifted to the UV region. After POM identifications, the thermal scheme of the blue phase range in the precursor VIS-PSBL during cooling procedure is N* 27.7˚C BP 42.9˚C ISO, and N* 33.8˚C BP 42.7˚C ISO in the heating procedure. [96] Meanwhile, the blue phase range in the precursor UV-PSBP during the cooling procedure is N* 42.5˚C BPI 45˚C BPII 49˚C ISO. The textures of VIS-PSBP mixture from 29˚C to 38˚C under POM observations are presented in Fig.

4.2. As for the UV-PSBP mixture, the POM observations are totally dark because the intrinsic reflection occurs in the UV region.

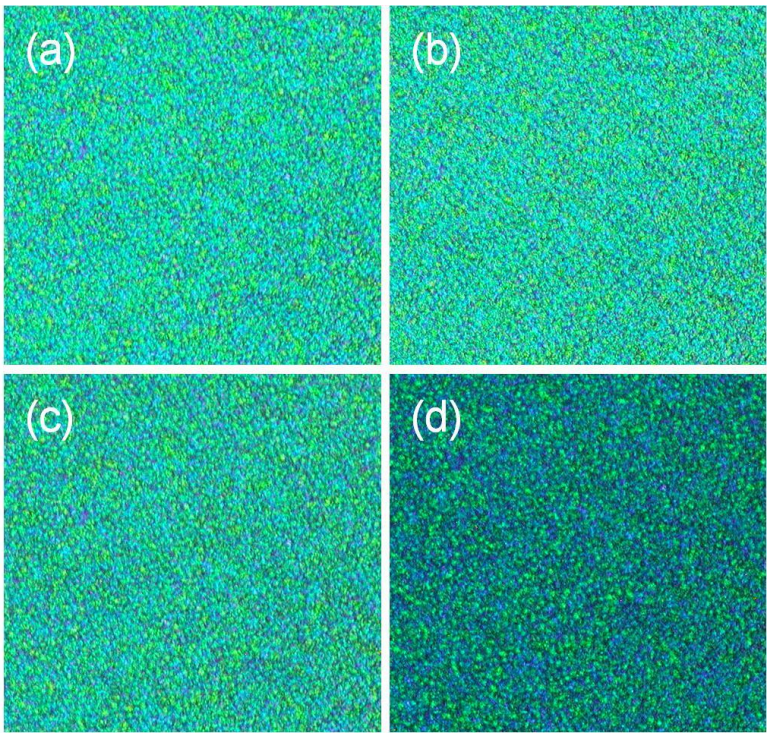

Figure 4.2 POM textures of sample VIS-PSBP at (a) 29˚C, (b) 32˚C, (c) 35˚C, and (d) 38˚C.

4.3 Polymerization Process

As indicated in reference [28], the photo-polymerization condition for a polymer-stabilized blue phase mixture is sensitive and complicated. According to the physical properties of the compositions in each system, different polymerization processes should be utilized and carefully optimized. In the cases of VIS-PSBP and UV-PSBP here, two polymerization approaches will be implemented. As found in section 4.2, the blue phase range of VIS-PSBP is

about 15-degree wide. With this wide temperature range, four fixed temperature points during the polymerization process were chosen to evaluate the impacts of the curing temperature effect on the POM morphology and the EO performance. The setup of the UV polymerization process is illustrated in Fig. 4.3.

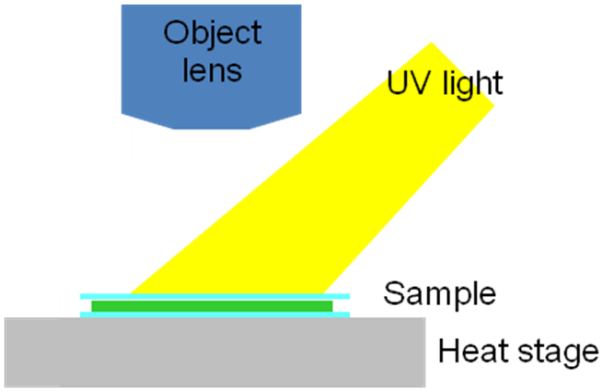

Figure 4.3 Setup of the polymerization process.

First, we started with the precursor VIS-PSBP. After stabilization at the designated temperature, two stages of UV light exposures were used (0.9 mW/cm^2, 20 min., and 2.6 mW/cm^2, 1 min.) to complete the photo-polymerization process. The POM observations at the room temperature of the polymer stabilized VIS-PSBP are shown in Fig. 4.4.

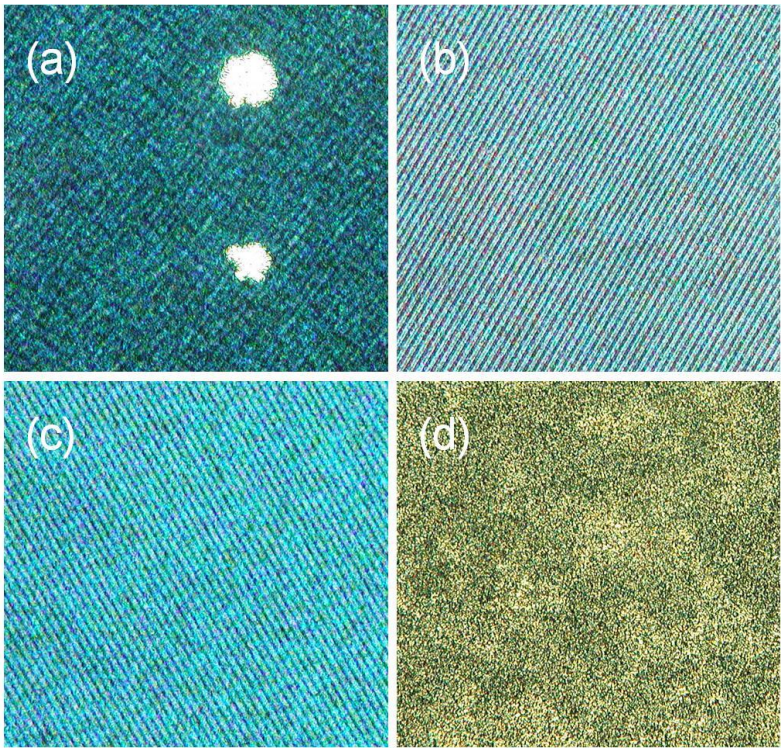

Figure 4.4 Room temperature POM textures of VIS-PSBP cured at (a) 29˚C, (b) 32˚C, (c) 35˚C, and (d) 38˚C.

In Fig. 4.4(a), the temperature during polymerization process was set at 29˚C, located in the super-cooling range of the blue phase state. After polymerization some regions were evolved into N* state and cured in-situ as the bright spots. On the other hand, while the VIS-PSBP precursor was polymerized in the opposite situation at the higher edge of the blue phase range, 38˚C, blue phase feature was not observed after the polymerization process as shown in the POM observation, Fig. 4.4(d). Except these two extreme cases presented above, blue phase texture was kept after polymerization when the curing temperature was chosen at the middle of the blue phase range as presented in Figs. 4.4(b) and 4.4(c). However, the pitch length was changed after polymerization comparing the color between Figs. 4.2(b), 4.2(c), and Figs. 4.4(b), 4.4(c),

respectively. The dark stripes in Figs. 4.4(b) and 4.4(c) are from the damage of the polymer network after several voltage operations. Based on the above very different POM textures of VIS-PSBP samples polymerized at different curing temperatures, distinct EO performance from these samples could also be expected.

In the second case, the precursor UV-PSBP was polymerized by the same setup in Fig. 4.3. However, because of the narrow blue phase temperature range, a more complicated curing process should be adopted. Based on the polymer kinetic, polymer precursor is a dynamic system during the polymerization process. Additionally, as indicated in reference [28], the stable temperature range of the blue phase state will expand and also shift at the same time with the progress of polymerization. Therefore, a two-step curing procedure with an ascending curing temperature (2˚C/20min) at the first step and a fixed temperature at the second step (10min) were implemented for the UV-PSBP precursor. Moreover, as found in section 4.2, two blue phase states were observed. Thus, two UV-PSBP samples were prepared by curing the precursor at BPI and BPII, respectively.

4.4 Electro-Optics of Polymer-Stabilized Blue Phase Liquid Crystal

After the polymerization process was completed, the EO performances of these polymer-stabilized blue phase samples were evaluated by the measurement setup employing two crossed polarizers and a He-Ne laser as described in chapter 3.

4.4.1 Polymer Stabilized VIS-BPLC

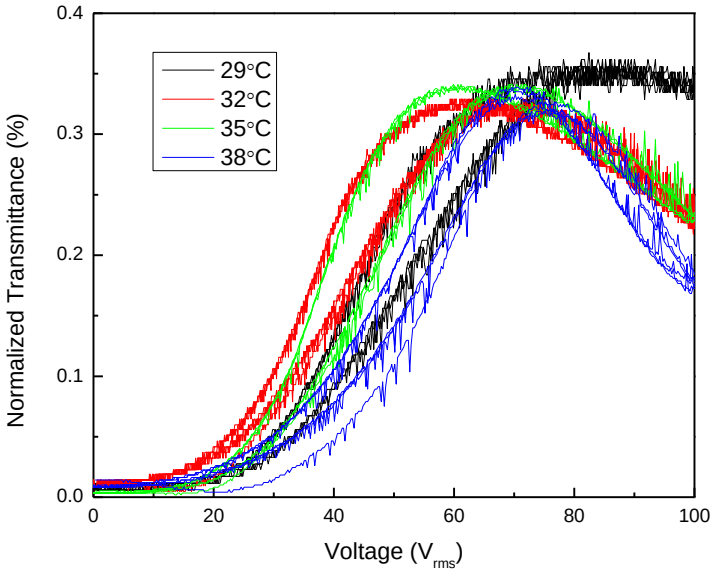

Figure 4.5 VT curves at room temperature of the VIS-PSBP samples cured at 29˚C, 32˚C, 35˚C, and 38˚C.

Fig. 4.5 depicts the measured VT curves of the VIS-PSBP samples at room temperature. Same voltage waveforms and duty cycles as described in chapter 3 were used. The peak voltage (V_p) of these VIS-PSBP samples is near $70V_{rms}$. However, the V_p of the two samples cured at either the lower (29˚C) or the higher (38˚C) edge is higher than that of the other two samples cured in the middle of the blue phase range (32˚C and 35˚C). Besides VT curves, distinct difference is also observed in the response time between these VIS-PSBP samples. Fig. 4.6 shows the full on-off response time of these four samples.

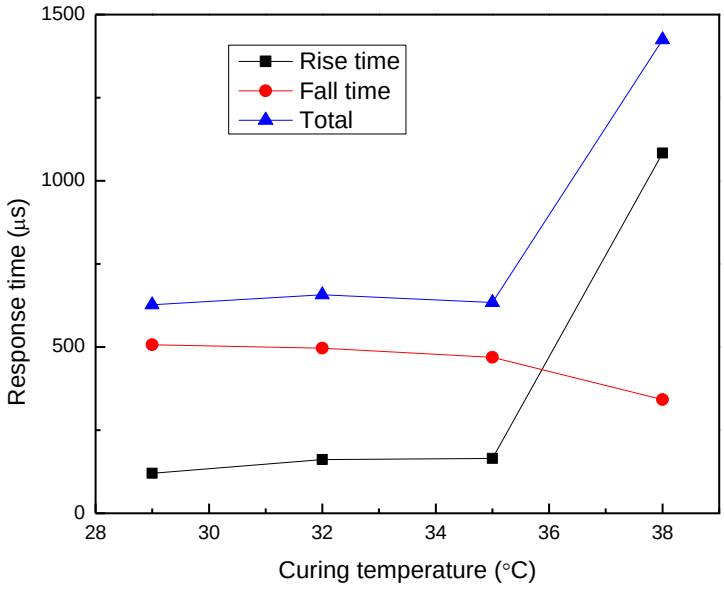

Figure 4.6 Full on-off response times of the VIS-PSBP samples cured at 29˚C, 32˚C, 35˚C, and 38˚C.

The full on-off response times in samples cured at 29˚C, 32˚C, and 35˚C are all below 1ms. Surprisingly, although operated under a higher voltage the response time from the sample cured at 38˚C is longer than other samples and over 1ms. From the above results, it shows that the curing temperature has a great impact to the EO performances of polymer-stabilized blue phase liquid crystal samples based on the same mixture. If a blue phase precursor has a narrow blue phase range like that in the second case, the UV-PSBP mixture, a more complex curing condition should be utilized in order to obtain good EO performance.

4.4.2 Polymer Stabilized UV-PSBP (Blue Phase I)

As mentioned before, for transmission-type display applications the colored reflection from the intrinsic blue phase pitch should be avoided. Thus, the EO features of the polymer-

stabilized BPLC with a reflection band in the UV region, such as UV-PSBP, should be used in practical applications. After stabilizing the UV-PSBP precursor at BPI state, the VT curves in UV-PSBPI by ascending and descending voltage operation cycles was measured and results are plotted in Fig. 4.7.

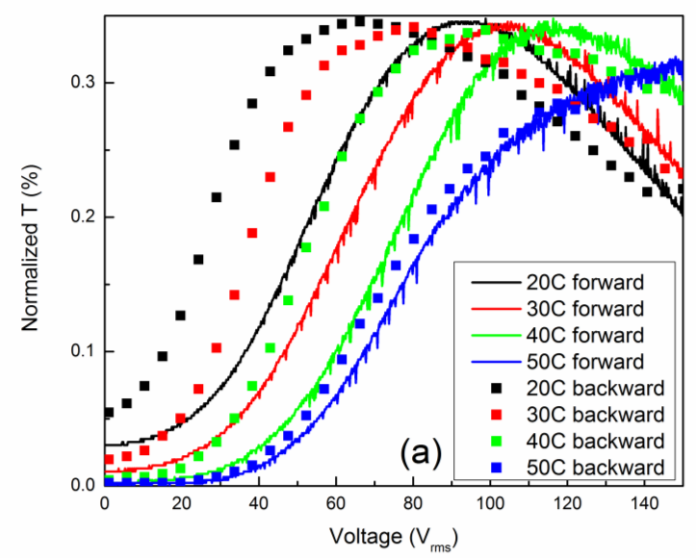

Figure 4.7 Measured VT curves of UV-PSBPI sample from 20˚C to 50˚C.

The peak transmittance voltage (V_p) shifts from ~90V_{rms} to ~120V_{rms} as the temperature increases from 20˚C to 40˚C. On the other hand, hysteresis becomes smaller with increased operation temperature. Fig. 4.8 shows the full on-off response time of UV-PSBPI operated at 45˚C.

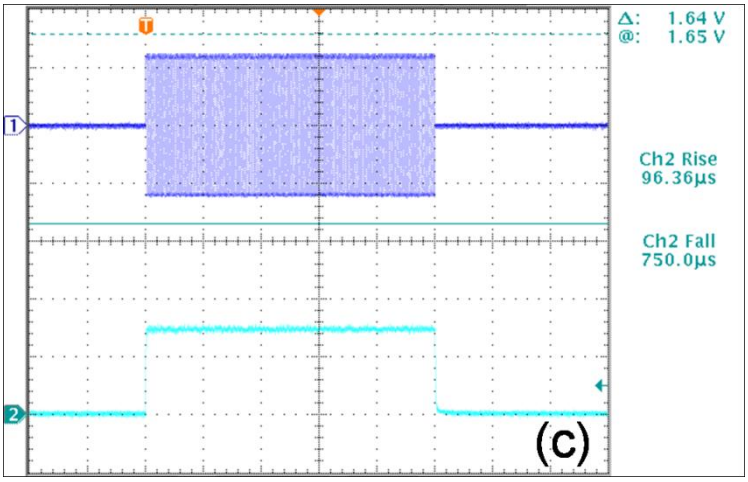

Figure 4.8 Measured full on-off response time of UV-PSBPI sample at 45˚C.

Different from the sample before polymerization, like UVBL operated at BPI, the response time of UV-PSBPI is one order faster and below 1ms. From the measured time domain optical response, different from the UVBL sample, only one mechanism was involved in the UV-PSBPI sample. Local molecular reorientation was believed as the main contribution here from the observed submillisecond response time. Therefore, some intrinsic BP features were suppressed, such as electrostriction and phase transition mechanisms, due to the existence of the polymer network structure. [28] Based on the above theory and evidence, the polymer/liquid crystal composite materials after polymerization process, such as UV-PSBP samples, should be considered as a different system from the liquid crystal only system. More details of the polymer/BPLC composite will be discussed in the following sections.

4.4.3 Polymer Stabilized UV-PSBP (Blue Phase II)

Based on the observations in section 4.2, another BP state, BPII, was found in the UV-PSBP precursor. Therefore, to study the difference between the polymer-stabilized samples at

these two blue phase states, another UV-PSBPII sample was prepared by curing the precursor at the BPII state. The ascending and the descending VT curves of UV-PSBPII sample from 20˚C to 50˚C were recorded in Fig. 4.9.

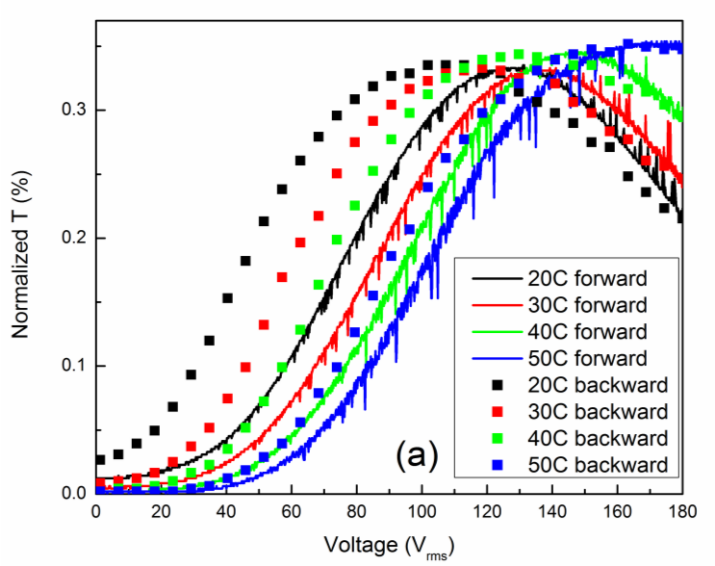

Figure 4.9 Measured VT curves of UV-PSBPII sample from 20˚C to 50˚C.

Compared to the VT curves in the UV-PSBPI sample, the peak transmittance voltage (V_p) of UV-PSBPII is higher than that of UV-PSBPI from about $130V_{rms}$ to $150V_{rms}$ when the operating temperature increases from 20˚C to 40˚C. But, the restored dark state is better than that of the UV-PSBPI sample. Also, the hysteresis problem is improved in the UV-PSBPII sample. However, if compared to the un-polymerized UVBL sample operated at the BPII state, the hysteresis phenomenon was deteriorated significantly.

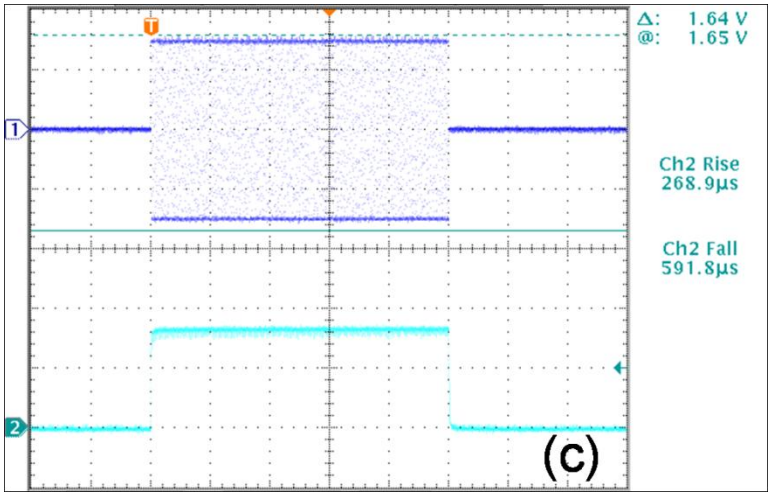

Figure 4.10 Measured full on-off response time of UV-PSBPII sample at 45˚C.

Fig. 4.10 presents the full on-off response time of the UV-PSBPII sample. The total response time is about 0.8ms. Compared to the blue phase system before polymerization, the change of response time is insignificant. From the lattice structures of the blue phase liquid crystal and based on the above time domain optical responses from samples in both BPI, BPII, and before and after polarization processes, some hypothesis can be proposed. First of all, the Kerr constant in BPI is higher than that of BPII in both before and after polymerization. Based on the molecular arrangement, the compactness of the LC stacking in BPII is less than that of BPI. Therefore, the LC stacking in BPII is closer to that of isotropic state than it is in BPI. As a result, the director of the LC clusters in BPI can be collectively moved more easily in a same direction than it is in the BPII state. Thus, the Kerr constant is higher in BPI. However, during the restoration to the initial BPI structure after the electric field is removed, it requires a longer time to go back to a more compact lattice structure than it needs in the BPII state. After polymerization, based on the formation of the polymer defect line theory [28], although polymer networks were formed in the defect lines after polymerization, the influence of the polymer

network to the liquid crystal molecular local movement (local molecular reorientation) is not huge. The defect clusters in the lattice structure are stabilized and fixed by the polymer network after polymerization. As a result, some intrinsic blue phase features, like electrostriction and phase transition, were suppressed after the formation of the polymer networks.

4.5 Gray Level Response Time in PSBP

Besides basic properties like VT curves and temperature performance, for display applications gray level response time is a critically important issue. From the viewpoint of measurement convenience and good dark state restoration, UV-PSBPII was used for the gray-level response studies. Fig. 4.11 shows the designated gray level voltages according to the VT curve when the sample was operated at 45˚C. Eight gray states at different transmittance levels were divided.

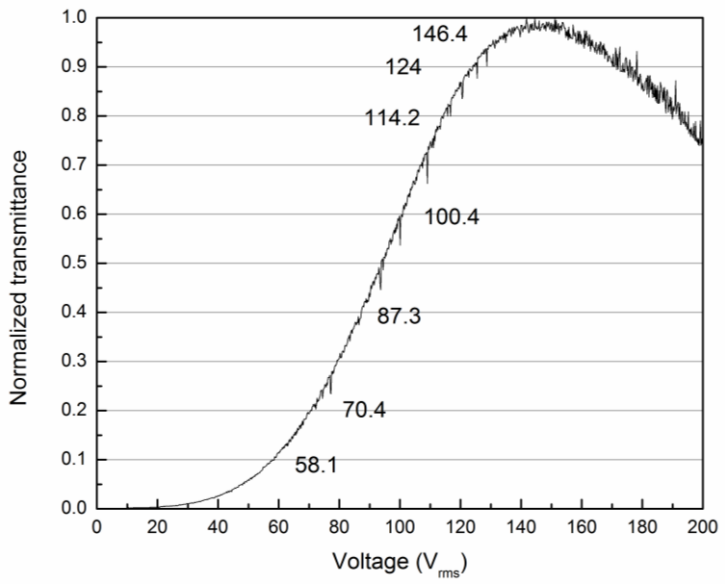

Figure 4.11 Gray level operating voltages of UV-PSBPII sample at 45˚C.

The measured response time between each gray level was collected in Table 4.1. Each gray level represents the normalized transmittance at the designated gray state. For example, T10 presents the gray level state of 10% of the maximum transmittance. The upper right triangle part in Table 4.1 is the rise time from a low gray level to a high gray level; while the lower left triangle is the fall time from high to low gray levels.

Table 4.1 Gray level response time.

	Rise time (μs)								
Fall time (μs)		T0	T10	T20	T40	T60	T80	T90	T100
	T0	X	370.6	208.4	57.6	58.6	57.4	57.6	56.9
	T10	282.2	X	526.0	162.2	121.9	122.4	100.2	57.8
	T20	262.5	307.1	X	300.4	271.4	227.5	156.2	56.6
	T40	341.0	279.8	208.6	X	342.7	357.7	296.6	31.6
	T60	376.8	259.8	197.7	253.8	X	247.9	350.9	251.4
	T80	337.4	313.9	283.7	343.3	202.9	X	185.6	367.3
	T90	381.4	258.1	191.4	223.5	259.0	172.2	X	273.5
	T100	367.5	376.0	344.0	372.8	149.5	321.4	347.9	X

As summarized in Table 4.1, the average rise and fall time between each gray level operation is about 300μs. To study the response time between gray level operations, the measured full on-off response time was evaluated by equations (3.7) and (3.8) first. The first row of the rise time and the first column of the fall time (between T0 and other gray levels) to the operating voltage were plotted in Fig. 4.12 and Fig. 4.13, respectively. According to the response time equation of a blue phase liquid crystal system in equation (3.7) and equation (3.8), the full-on time (rise time) is dependent to the applied voltage while the full-off time (fall time) is independent of the operating voltage. After fitting equation (3.8) with the measured rise time, the fitting curve is drawn as the red line in Fig. 4.12. Two other fitting parameters, critical voltage (V_c) and fall time (τ_{fall}), can also be found as 42.8V_{rms} and 315.9μs. Comparing the measured

average fall time, 336μs in Fig. 4.13, to the fitted fall time from the response time equations, the measured results match quite well to the equations proposed by Gleeson and Coles. [83]

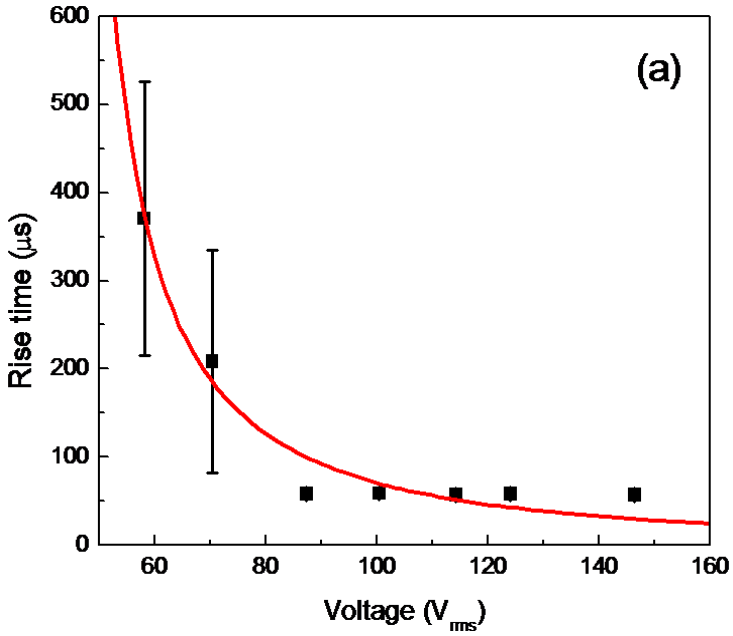

Figure 4.12 Measured rise time between T0 and other gray levels.

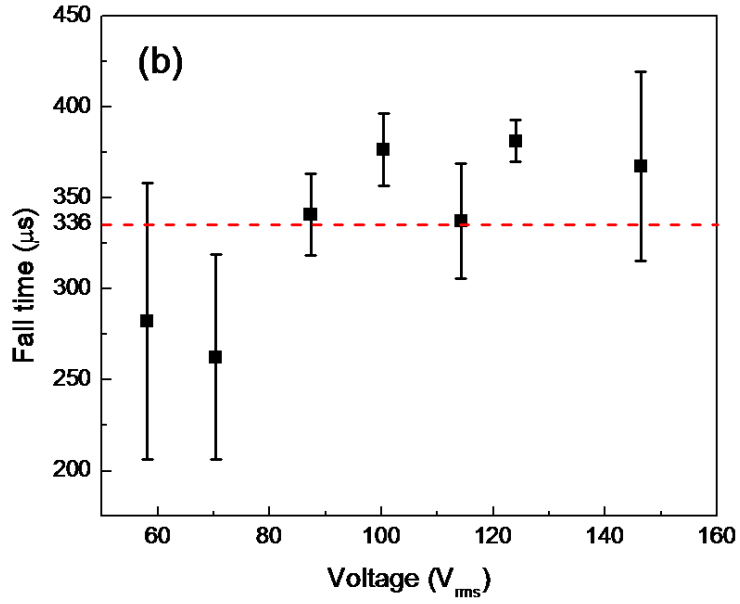

Figure 4.13 Average fall time between T0 and other gray levels.

In the following part, the gray level response time between T10 and other gray levels was studied. Fig. 4.14 and Fig. 4.15 plot the rise time and the fall time between T10 and other higher gray level states according to the second row and the second column in Table 4.1.

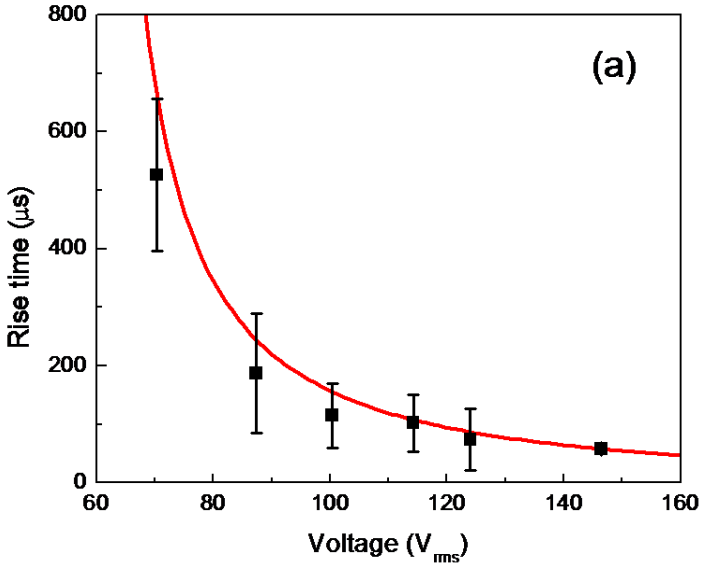

Figure 4.14 Measured rise time between T10 and other gray levels.

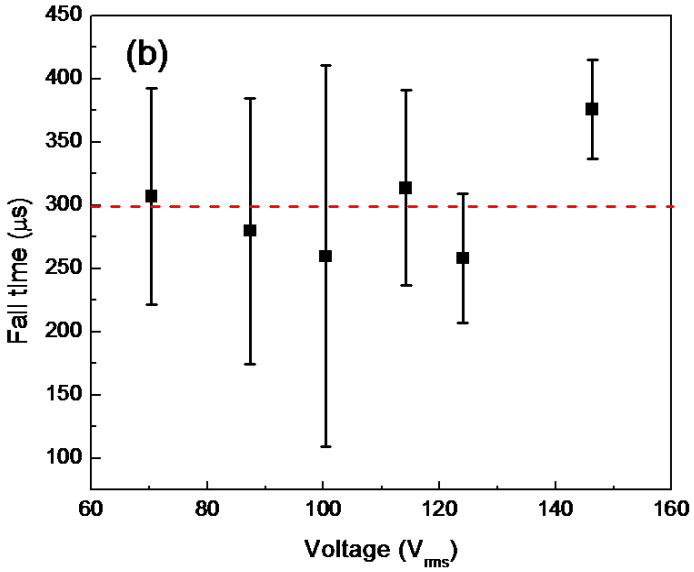

Figure 4.15 Average fall time between T10 and other gray levels.

Analogous to the concept used in the gray level response time of a nematic liquid crystal device, [97] we propose a bias voltage (V_b) to describe the gray level response time equations for a blue phase liquid crystal system. Based on equation (3.7) and (3.8), the gray level response time for BPLC can be rewritten as

$$\tau_{off} = \frac{\gamma_1}{E_c^2 \varepsilon_0 \Delta\varepsilon}, \tag{4.1}$$

$$\tau_{rise} = \frac{\tau_{off}}{\left(\frac{V}{V_b}\right)^2 - 1}, \tag{4.2}$$

Similar to the bias voltage in the nematic liquid crystal devices, the operating voltage of the gray level T10, 58.1V_{rms}, was set as the bias voltage in equation (4.2) for the gray level operations between T10 and other gray levels. After fitting the measured response time in Table 4.1 to equation (4.2), a fitted fall time was calculated as 308.3μs. Comparing to the measured average fall time from table 4.1, 299.1μs, the fitted fall time is within the experimental error.

4.6 Electrode Dimension Effect

So far, the above shown operating voltages of a BPLC system were all about 100V_{rms}, which makes BPLC impractical for display applications. To satisfy the basic display criteria, the electric field induced birefringence should be large enough to reach a phase retardation of one π at an acceptable voltage. According to Gerber and Singh, the induced birefringence (δn) in a BPLC system is proportional to the square of the electric field and related to the material

parameters in the system as [98]

$$\delta n \approx \Delta n \Delta\varepsilon \frac{\varepsilon_0}{K_2 q^2} E^2, \tag{4.3}$$

where Δn is the birefringence, $\Delta\varepsilon$ the dielectric anisotropy, K_2 the twist elastic constant, and $q=\pi/p$, the inverse of the pitch length.

As a result, there are two possible directions to reduce the operating voltage in a BPLC system. One of them is to increase the birefringence, dielectric anisotropy or pitch length of a BPLC system. However, modifications of the material parameters in the system usually cause the blue phase state to disappear or even lead to an unstable material. So far, the largest Kerr constant (K~13 nm/V^2) BPLC composite was reported by the UCF/Chisso group. [35] The EO performance of this material will be discussed later in this section. The other approach to lower the operating voltage is to increase the effective strength and the affecting volume of the electric field. Several approaches have shown the potentials for reducing the required operating voltage. [31]-[34] Here in this section, we also demonstrate another viable approach to reduce the operating voltage.

Generally speaking, the Kerr constant of a BPLC material system is at the level of 0.1nm/V^2 if the LC birefringence is ~0.15 and dielectric anisotropy ~10. In the high Kerr constant BPLC material from Chisso, the LC birefringence is 0.17 and the dielectric anisotropy as high as 94. After using this high Kerr constant material, the operating voltage was dramatically reduced from ~100V$_{rms}$ to ~50V$_{rms}$ in an IPS electrode of 10-μm electrode width and 10-μm electrode spacing. To further reduce the operating voltage, increasing the electric field strength and penetration depth can also be considered. Based on this high Kerr constant

BPLC material, a stronger electric filed induced by a smaller electrode width and spacing was evaluated.

Fig. 4.16 shows the VT curves in different electrode dimension with this Chisso BPLC material. The detected transmittance is normalized to the total transmittance when the BPLC sample was measured under parallel and crossed polarizers. Four configurations of the electrode width and spacing were compared. When the sample was operated under a same temperature, the peak transmittance voltage decreased with a smaller electrode width and spacing. The operating voltage was decreased to $40V_{rms}$ at 25˚C when the electrode width and spacing were reduced to 2μm and 4μm. Another interesting observation is that the maximum transmittance stays over 80% even in a smaller electrode, which is a relief to the concern of transmittance reduction and also very different from the simulation prediction. [31]

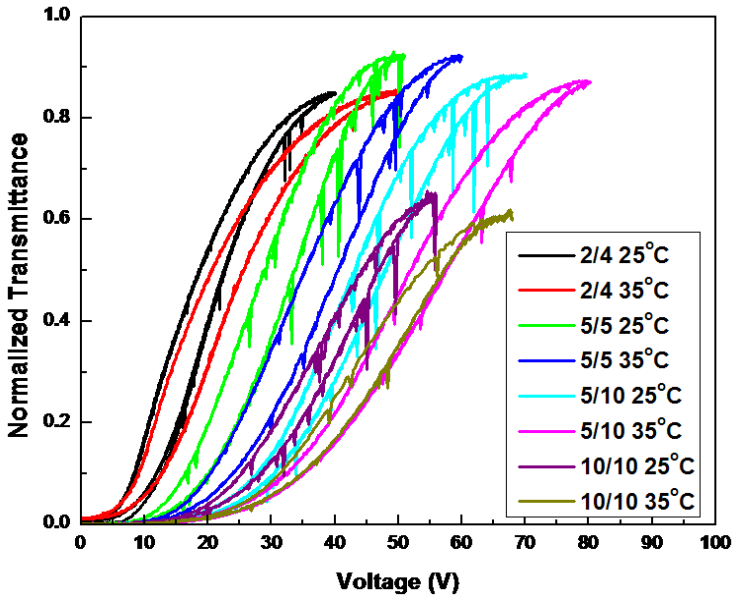

Figure 4.16 Measured VT curves of the high Kerr constant BPLC material with different electrode dimension at 25˚C and 35˚C, λ=633nm.

Fig. 4.17 summarizes the peak transmittance voltage and the hysteresis in these electrode configurations. As shown, except the 10/10 case the hysteresis problem is mitigated when the dimension of the electrode gets larger. The reduction of the stress on the polymer network induced by the electric field might be the main reason. Detail observations will be discussed in the later part.

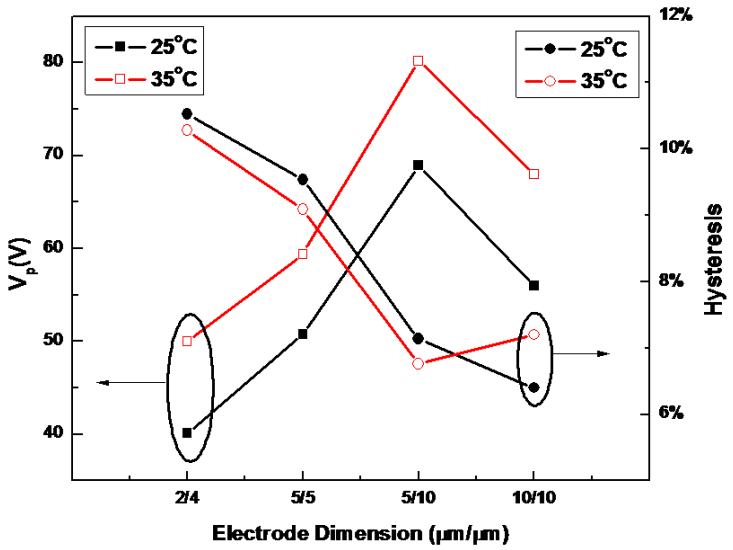

Figure 4.17 Measured peak transmittance voltage and hysteresis of the high Kerr constant BPLC in Fig. 4.16.

Fig. 4.18 shows the full on-off response time from the sample with different electrode dimensions. Except the sample with 2/2 electrode, the full on-off response time in other samples are in the level of 2ms. Overall speaking, the response time becomes faster in a smaller electrode dimension. As an exception for the 2/2 electrode, the polymer network deformation induced phase transition caused by strong electric field might be the reason. Further discussions will be given in the following part with more detailed POM observations.

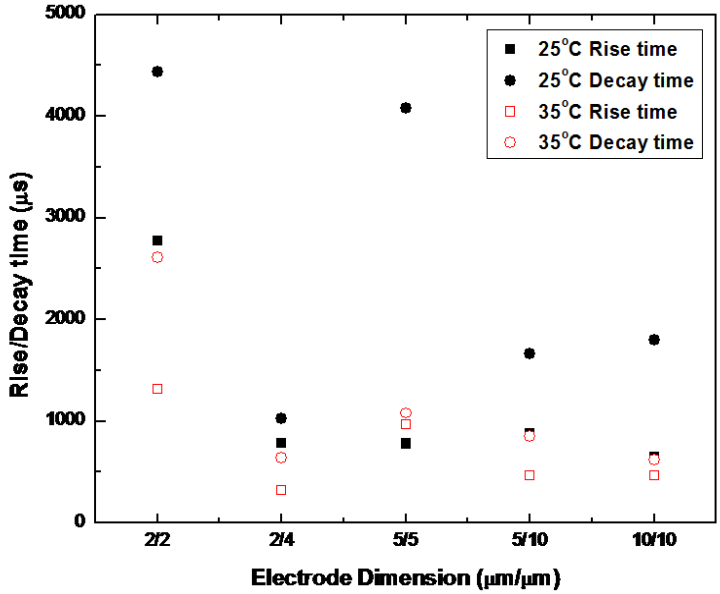

Figure 4.18 Measured fall on-off response time of the high Kerr constant BPLC at 25˚C and 35˚C.

POM observations of the LC textures at different conditions are presented in Fig. 4.19. When a voltage was applied to the BPLC sample, the LC molecules were reoriented along the electric field which in turn induces an optical birefringence. Therefore, a bright state can be observed with a proper orientation of the sample to the polarizers. Figs. 4.19(a) and 4.19(b) show the bright state at the peak transmittance voltage V_p under POM observations from the sample with the 5/5 and 10/10 electrode respectively. The black area in the figure is the location of the electrode; while the bright area is the spacing between the electrode fingers. In the 10/10 electrode, Fig. 4.19(b), the ratio of the bright and the dark region is about 1 to 1, which is close to the measured peak normalized transmittance in Fig. 4.16. However, the ratio of the bright region to the whole area of the 5/5 sample in Fig. 4.19(a) is estimated to be about 70%.

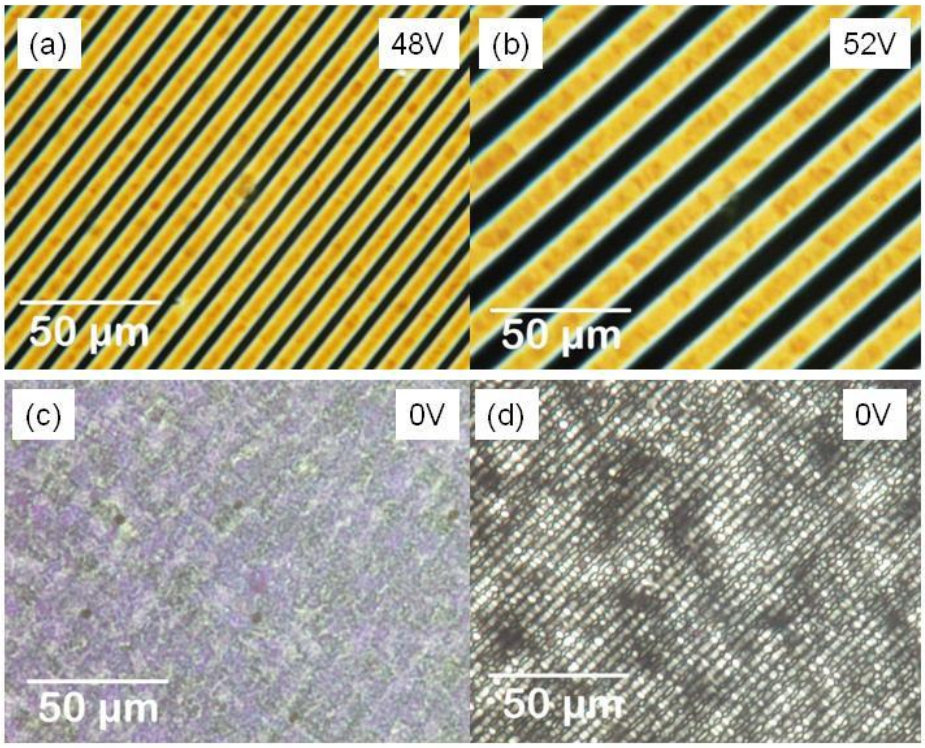

Figure 4.19 POM observations of the samples with (a) 5/5, and (b) 10/10 electrodes at the specified peak voltage; (c) 5/5, and (d) 2/2 electrode at V=0 after voltage operation.

Although the ratio of the electrode width and the spacing is the same in the 5/5 and in the 10/10 sample the transmittance at related V_p is totally different. As shown in POM pictures, the bright area infiltrates further into the electrode region in the 5/5 case, which indicates more LC molecules within the electrode region were affected by the strong electric field compared to that of the sample with 10/10 electrode. This surprisingly high transmittance in the sample with smaller electrodes becomes an advantage as it overcomes the low transmittance problem predicted by the simulation works.

However, there is limitation in reducing the electrode dimension. As presented in Figs. 4.19(c) and (d), the POM pictures were taken from the samples with 5/5 and 2/2 electrodes after voltage operations respectively. In the 5/5 sample, although some fiber-like white textures were observed under the POM, in most of the area the texture of the sample was still in the blue phase state. On the contrary, after voltage operation the blue phase texture in the 2/2 sample was destroyed as shown in Fig. 4.19(d). Therefore, phase transition occurs after voltage operation in the 2/2 sample and the response time also became longer than other cases.

4.7 Summary

To prove the feasibility of BPLC materials for display applications, attempts in different aspects from the stabilization of blue phase system, the avoidance of colored reflection, to the reduction of operating voltage by either improving material systems or electric field strength by different electrode dimension are discussed. Different polymer stabilization processes are conducted according to the condition of each blue phase liquid crystal mixture. Also, the difference between the same polymerization procedure at different temperature or blue phase state is discussed. Depending on the polymerization condition, different EO performance is obtained though based on one same blue phase liquid crystal mixture. After analyzing the EO performance of the PSBP samples, we develop a physical model to describe the gray level operations of the PS-BPLC. Besides response time, hysteresis in the polymer-stabilized BPLC is different from that in the BPLC system. Therefore, polymer-stabilized BPLC possesses some different EO features and should be discussed separately.

At the last part, attempts for low voltage BPLC samples were investigated. Until now, the

measured operating voltage is reduced to about $40V_{rms}$ by integrating Chisso's high Kerr constant BPLC material into an IPS cell with 2-μm electrode width and 4-μm electrode gap. Further developments in new BPLC materials and optimization of device structures are undertaking by Chisso, Merck, and several other research groups worldwide. Thus, in a foreseeable near future it is promising to achieve BPLC displays with a fairly low driving voltage (<10V) while keeping submillisecond response time.

CHAPTER 5: CONCLUSION

Among the fast-response liquid crystal display technologies, blue phase liquid crystal is a promising candidate. In this dissertation, the feasibility and the characteristics of blue phase liquid crystal display are investigated from material systems to EO performances under different test cells.

From the material system investigations in chapter 2, various blue phase liquid crystal systems were considered. A viable blue phase liquid crystal system for further improvements was developed by different evaluation approaches. Based on these evaluations, various criteria of the compositions for a blue phase liquid crystal system should be taken into considerations, such as miscibility, stability, applicable temperature range, etc. Generally speaking, to achieve a desired EO performance, several liquid crystal material properties are desired, such as, low viscosity, high birefringence, high dielectric anisotropy, and wide stable temperature range for the blue phase state. However, these desired features are usually contradicted to each other. For examples, high dielectric anisotropy material usually has a high viscosity; high birefringence material is usually unstable; and etc. As a result, the balance of each component in the system becomes a key issue.

To characterize the EO performance of the blue phase liquid crystal, the samples developed in chapter 2, chapter 3, and from Chisso were evaluated in different test cells. As described in chapter 3 and chapter 4, the response time can be reduced to ~300μs in a PS-BPLC

cell which is about one order of magnitude faster than the conventional nematic liquid crystal. Equations governing the response time between different gray levels are also proposed and test cells characterized. However, the required operating voltage for this PS-BPLC sample is at the level of 100V which is too high to be practical for display applications. By utilizing a high Kerr constant blue phase liquid crystal material from Chisso, the operating voltage can be reduced to about 40V in an IPS cell with an electrode of 2μm in width and 4μm in spacing. However, comparing to the normal nematic liquid crystal displays, further reduction of the operating voltage is still needed. To achieve this goal, new material systems and new driving approaches need to be developed. With the improvements in high Kerr constant material, strong electric field, and deeper electric field penetration, a low-voltage blue phase liquid crystal display could be achieved in the near future.

In conclusion, in this dissertation we have developed a workable blue phase liquid crystal material. After evaluating the blue phase liquid crystal systems based on the prepared materials, some newly discovered BPLC properties are summarized as follows:

1. The EO properties, such as Kerr constant, response speed, hysteresis, etc are different in each blue phase states. For instance, in the BPI state, although the operating voltage is relatively low, the response time is slow, which is about 40ms, and the observed hysteresis is large, which is about 18%. However, in the BPII state, although the operating voltage is relatively high, the response time is fast, which is about 160μs, and no hysteresis is observed.
2. After polymerization, the PS-BPLC composite has entirely different EO properties because of the introduction of the polymer networks. The operating voltage in the PS-

BPLC system has the same trend as it in the system without polymer stabilization, i.e., the operating voltage is somewhat lower in the PS-BPI state than that in the PS-BPII. However, the response time and the hysteresis do not follow the same trend in the blue phase system without polymer networks. As depicted in this dissertation, the response time in the PS-BPLC at both PS-BPI state and PS-BPII state can be reduced to about 800μs. However, the hysteresis issue shows up in the PS-BPLC at both BP states, which are 12.2% in PS-BPI at 45℃ and 11.8% in PS-BPII at 45℃.

3. The overall total response time of the dynamic operations between different gray scales is confirmed at the level of submillisecond.
4. The equations to describe the dynamic behaviors of the blue phase in gray scale operations are proposed and validated. According to these equations, the gray scale response time of a blue phase material can be estimated by the material parameters and the condition of the driving voltage. Also, these equations indicate the possibility of a faster response time by further utilizing either the overdrive or the undershoot operation or both in the PS-BPLC system.

We believe this work paves useful guidelines to a better blue phase liquid crystal display.

LIST OF REFERENCES

[1] G. H. Wagniere, *On chirality and the universal asymmetry: reflections on image and mirror image* (Wiley, New York, 2007).

[2] B. E. A. Saleh and M. C. Teich, *Fundamentals of Photonics* (Wiley, New York, 1991).

[3] P. M. Knoll and H. Kelker, *O. Lehmann: Researcher of the Liquid Crystals* (Books on Demand GmbH, Norderstedt, 2010).

[4] Liquid crystal (www.wikipedia.org).

[5] S. T. Wu and D. K. Yang, *Reflective Liquid crystal Displays* (Wiley, New York, 2005).

[6] H. Xianyu, K. M. Chen, and S. T. Wu, *J. Soc. Info. Display* **16**, 125 (2008).

[7] Q. Hong, T. X. Wu, and S. T. Wu, *Liq. Cryst.* **30**, 367 (2003).

[8] G. Gottarelli and G. P. Spada, *Mol. Cryst. Liq. Cryst.* **123**, 377 (1985).

[9] V. A. Belyakov and V. E. Dmitrienko, *Sov. Phys. Usp.* **28**, 535 (1985).

[10] O. Lehmann, *Zeitschrift fur Physikalische Chemie* **56**, 750 (1906).

[11] G. W. Gray, *J. Chem. Soc.* 3733 (1956).

[12] D. Armitage and F. P. Price, *J. Phys. (Paris)* **36**, C1-133 (1975).

[13] K. Bergmann and H. Stegemeyer, *Z. Naturforsch.* **34a**, 251 (1979).

[14] S. Meiboom and M. Sammon, *Phys. Rev. Lett.* **44**, 882 (1980); *Phys. Rev. A* **24**, 468 (1981).

[15] D. L. Johnson, J. H. Flack, and P. P. Crooker, *Phys. Rev. Lett.* **45**, 641 (1980); *Phys. Lett. A* **82**, 247 (1981).

[16] H. –S. Kitzerow and C. Bahr, *Chirality in Liquid Crystals* (Springer, New York, 2001).

[17] E. Dubois-Violette and B. Pansu, *Mol. Cryst. Liq. Cryst.* **165**, 151 (1988).

[18] P. Pieranski, E. Dubois-Violette, F. Rohten, and L. Strelecki, *J. Phys.* **42**, 53 (1981).

[19] W. F. Brinkman and P. E. Cladis, *Physics Today* **35**, 48 (1982).

[20] S. Meiboom, J. P. Sethna, P. W. Anderson, and W. F. Brinkman, *Phys. Rev. Lett.* **46**, 1216 (1981).

[21] S. Meiboom, M. Sammon, and W. F. Brinkman, *Phys. Rev. A* **27**, 438 (1983).

[22] S. Meiboom, M. Sammon, and D. W. Berreman, *Phys. Rev. A* **28**, 553 (1983).

[23] J. P. Sethna, *Phys. Rev. B* **31**, 6278 (1985).

[24] H. J. Coles and M. N. Pivnenko, *Nature* **436**, 997 (2005).

[25] A. Yoshizawa, M. Sato and J. Rokunohe, *J. Mater. Chem.* **15**, 3285 (2005).

[26] H. Yoshida, Y. Tanaka, K. Kawamoto, H. Kubo, T. Tsuda, A. Fujii, S. Kuwabata, H. Kikuchi, M. Ozaki, *Appl. Phys. Express* **2**, 121501 (2009).

[27] E. Karatairi, B. Rozic, Z. Kutnjak, V. Tzitzios, G. Nounesis, G. Cordoyiannis, J. Thoen, C. Glorieux, and S. Kralj, *Phys. Rev. E* **81**, 041703 (2010).

[28] H. Kikuchi, M. Yokota, Y. Hisakado, H. Yang, and T. Kajiyama, *Nat Mater* **1**, 64 (2002).

[29] H. Kikuchi, Y. Haseba, S. Yamamoto, T. Iwata, and H. Higuchi, *SID Symposium Digest* **40**, 578 (2009).

[30] T. Iwata, K. Suzuki, H. Higuchi, and H. Kikuchi, *Liq. Cryst.* **36**, 947 (2009).

[31] L. Rao, Z. Ge, S. T. Wu, and S. H. Lee, *Appl. Phys. Lett.* **95**, 231101 (2009).

[32] S. Yoon, M. Kim, M. S. Kim, B. G. Kang, M. K. Kim, A. K. Srivastava, S. H. Lee, Z. Ge, L. Rao, S. Gauza, and S. T. Wu, *Liq. Cryst.* **37**, 201 (2010).

[33] M. Jiao, Y. Li, and S. T. Wu, *Appl. Phys. Lett.* **96**, 011102 (2010).

[34] H. C. Cheng, J. Yan, T. Ishinabe, and S. T. Wu, *Appl. Phys. Lett.* **98**, 261102 (2011).

[35] K. M. Chen, J. Yan, S. T. Wu, Y. P. Chang, C. C. Tsai, and J. W. Shiu, *J. Display Technol.* **7**, 362 (2011).

[36] H. Lee, H. –J. Park, O. –J. Kwon, S. J. Yun, J. H. Park, S. Hong, and S. –T. Shin, *SID Symposium Digest* **42**, 121 (2011).

[37] Y. Hirakata, D. Kubota, A. Yamashita, H. Miyake, M. Hayakawa, J. Koyama, S. Yamazaki, K. Okazaki, R. Sato, T. Cho, K. Tochibayashi, and M. Sakakura, *SID Symposium Digest* **42**, 32 (2011).

[38] K. M. Chen, S. Gauza, H. Xianyu, and S. T. Wu, *J. Display Technol*. **6**, 318 (2010).

[39] C. –Y. Fan, C. –T Wang, T. –H. Lin, F. –C. Yu, T. –H. Huang, C. –Y. Liu, and N. Sugiura, *SID Symposium Digest* **42**, 213 (2011).

[40] J. Yan and S. T. Wu, *SID Symposium Digest* **42**, 210 (2011).

[41] M. Schadt and W. Helfrich, *Appl. Phys. Lett.* **18**, 127 (1971).

[42] R. A. Soref, J. *Appl. Phys.* **45**, 5466 (1974).

[43] M. Oh-e, M. Yoneya, and K. Kondo, *J. Appl. Phys*. **82**, 528 (1997).

[44] M. F. Schiekel and K. Fahrenschon, *Appl. Phys. Lett.* **19**, 391 (1971).

[45] A. Takeda, S. Kataoka, T. Sasaki, H. Chida, H. Tsuda, K. Ohmuro, T. Sasabayashi. Y. Koike, and K. Okamoto, *SID Symposium Digest* **29**, 1077 (1998).

[46] S. H. Lee, S. L. Lee, and H. Y. Kim, *Appl. Phys. Lett.* **73**, 2881 (1998).

[47] J. H. Lee, X. Zhu, and S. T. Wu, *J. Display Technol*. **3**, 2 (2007).

[48] Z. Ge, L. Rao, S. Gauza, and S. T. Wu, *J. Display Technol*. **5**, 250 (2009).

[49] G. D. Love, *Appl. Opt.* **32**, 2222 (1993).

[50] S. T. Wu and C. S. Wu, *J. Appl. Phys.* **65**, 527 (1989).

[51] H. Ono and N. Kawatsuki, *Appl. Phys. Lett*. **71**, 1162 (1997).

[52] S. T. Kowel, D. S. Cleverly, and P. G. Kornreich, *Appl. Opt.* **23**, 278 (1984).

[53] M. Ye, B. Wang, and S. Sato, *Opt. Commun.* **259**, 710 (2006).

[54] G. D. Love, *Appl. Opt.* **36**, 1517 (1997).

[55] J. L. West, U.S. Patent No. 5004323 (2 April 1991).

[56] A. Miyamoto, H. Kikuchi, S. Kobayashi, Y. Morimura, and T. Kajiyama, *Macromolecules* **24**, 3915 (1991)

[57] T. Matsui, R. Ozaki, K. Funamoto, M. Ozaki, and K. Yoshino, *Appl. Phys. Lett*. **81**, 3741 (2002).

[58] S. T. Wu, A. M. Lackner, and U. Efron, *Appl. Opt.* **26**, 3441 (1987).

[59] D. Coates, *J. Mater. Chem.* **5**, 2063 (1995).

[60] R. L. Sutherland, L. V. Natarajan, V. P. Tondiglia, S. Chandra, C. K. Shepherd, D. M. Brandelik, S. A. Siwecki, and T. J. Bunning, *J. Opt. Soc. Am. B* **19**, 3004 (2002)

[61] I. Fujieda, *Appl. Opt.* **34**, 6252 (2001).

[62] S. A. Carter, J. D. LeGrange, W. White, J. Boo, and P. Wiltzius, *J. Appl. Phys.* **81**, 5992 (1997).

[63] J. B. Nephew, T. C. Nihei, and S. A. Carter, *Phys. Rev. Lett.* **80**, 3276 (1998).

[64] G. M. Russell, B. J. A. Paterson, C. T. imrie, and S. K. Heeks, *Chem. Mater.* **7**, 2185 (1995)

[65] C. C. Bowley, P. A. Kossyrev, G. P. Crawford, and S. Faris, *Appl. Phys. Lett*. **79**, 9 (2001).

[66] M. Jazbinsek, I. D. Olenik, M. Zgonik, A. K. Fontecchio, and G. P. Crawford, *J. Appl. Phys.*

90, 3831 (2001).

[67] H. Ren and S. T. Wu, *Opt. Express* **14**, 11292 (2006).

[68] H. Okada, P. J. Bos, and H. Onnagawa, *Jpn. J. Appl. Phys.* **37**, 2576 (1998).

[69] Q. Wang, D. Zhang, Y. Huang, Z. Ni, J. Chen, Y. Zhong, and S. Zhuang, *Opt. Lett.* **35**, 1236 (2010).

[70] K. Kang and S. Sprunt, *Phys. Rev. E* **72**, 031702 (2005).

[71] S. –L. Wu and W. –J. Hsieh, *Liq. Cryst.* **21**, 783 (1996).

[72] J. Thoen, *Phys. Rev. A* **37**,1754 (1988).

[73] U. Singh and P. H. Keyes, *Liq. Cryst.* **8**, 851 (1990).

[74] D. C. Wright and N. D. Mermin, *Rev. Mod. Phys.* **61**, 385 (1989).

[75] H. –S. Kitzerow, *Ferroelectrics* **395**, 66 (2010).

[76] D. Armitage and R. J. Cox, *Mol. Cryst. Liq. Cryst.* **64**, 41 (1980).

[77] H. –S. Kitzerow, *Mol. Cryst. Liq. Cryst.* **202**, 51 (1991).

[78] M. Sato and A. Yoshizawa, *Adv. Mater.* **19**, 4145 (2007).

[79] H. –S. Kitzerow, P. P. Crooker, S. L. kwok, J. Xu, G. Heppke, *Phys. Rev. A* **42**, 3442 (1990).

[80] V. K. Dolganov, G. Heppke, and H. –S. Kitzerow, *J. Phys. II France* **2**, 1803 (1992).

[81] H. –S. Kitzerow, P. P. Crooker, J. Rand, J. Xu, G. Heppke, *J. Phys. II France* **2**, 279 (1992).

[82] H. J. Coles and H. F. Gleeson, *Mol. Cryst. Liq. Cryst.* **167**, 213 (1989).

[83] H. F. Gleeson and H. J. Coles, *Liq. Cryst.* **5**, 917 (1989).

[84] G. Heppke, B. Jerome, H. –S. Kitzerow, P. Pieranski, *J. Phys. France* **50**, 549 (1989).

[85] G. Heppke, B. Jerome, H. –S. Kitzerow, P. Pieranski, *J. Phys. France* **50**, 2991 (1989).

[86] F. Porsch, H. Stegemeyer, and K. Hiltrop, *Z. Naturforsch.* **39a**, 475 (1984).

[87] J. F. Nye, *Physical Properties of Crystals* (Clarendon Press, Oxford, 1989).

[88] B. E. A. Saleh and M. C. Teich, *Fundamentals of Photonics* (John Wiley & Sons Inc., New York, 1991).

[89] M. Born and E. Wolf, *Principles of Optics* (Cambridge University Press, Cambridge, 1999).

[90] Hysteresis (www.wikipedia.org).

[91] P. S. Drzaic, *Liquid Crystal Dispersions* (World Scientific, Singapore, 1995).

[92] V. E. Dmitrienko, *Liq. Cryst.* **5**, 847 (1989).

[93] E. Jakeman and E. P. Raynes, *Phys. Lett.* **39A**, 69 (1972).

[94] H. Xianyu, Y. Zhao, S. Gauza, X. Liang, and S. T. Wu, *Liq. Cryst.* 3**5**, 1129 (2008).

[95] H. Kikuchi, H. Higuchi, Y. Haseba, and T. Iwata, *SID Symposium Digest* **38**, 1737 (2007).

[96] K. M. Chen, S. T. Wu, P. J. Hsieh, S. H. Liu, K. L. Cheng, C. C. Tsai, and J. W. Shiu, *IDMC*, S11-02 (2011).

[97] S. T. Wu, *Appl. Opt.* **28**, 48 (1989).

[98] P. R. Gerber, *Mol. Cryst. Liq. Cryst.* **116**, 197 (1985).

LIST OF STUDENT's PUBLICATIONS

Journal Publications:

[1] H. Xianyu, K. M. Chen, and S. T. Wu, "Flexible area-color reflective displays based on electric-field induced blueshift in a cholesteric liquid-crystal film" *J. SID* **16**, 125-128 (Jan. 2008).

[2] Y. J. Lin, K. M. Chen, and S. T. Wu, "Broadband and polarization-independent beam steering using dielectrophoresis-tilted prism" *Opt. Express* **17**, 8651-8656 (2009).

[3] K. M. Chen, H. Ren, and S. T. Wu, "PDLC-based VOA with a small polarization dependent loss" *Optics Commun.* **282**, 4374-4377 (2009).

[4] K. M. Chen, S. Gauza, H. Xianyu, and S. T. Wu, "Submillisecond gray-level response time of a polymer-stabilized blue phase liquid crystal" *J. Display Technol.* **6**, 49-51 (2010).

[5] K. M. Chen, S. Gauza, H. Xianyu, and S. T. Wu, "Hysteresis effects in blue-phase liquid crystals" *J. Display Technol.* **6**, 318-322 (2010).

[6] L. Rao, Z. Ge, S. Gauza, K. M. Chen, and S. T. Wu, "Emerging liquid crystal displays based on the Kerr effect," *Mol. Cryst. Liq. Cryst.* **527**, 30-42 (Aug. 2010).

[7] K. M. Chen, J. Yan, S. T. Wu, Y. P. Chang, C. C. Tsai, and J. W. Shiu, "Electrode dimension effects on blue-phase liquid crystal displays," *J. Display Technol.* **7**, 362 (2011).

Conference Proceedings:

[1] K. M. Chen, S. Gauza, H. Xianyu, and S. T. Wu, "Submillisecond gray-to-gray response time of polymer-stabilized blue-phase liquid crystals", SID Symposium Digest, **41**, 173 (2010).

[2] K. M. Chen, S. T. Wu, P. J. Hsieh, S. H. Liu, K. L. Cheng, C. C. Tsai, and J. W. Shiu, “Curing temperature effects on polymer-stabilized blue phase liquid crystals”, IDMC, S11-02 (2011).